MedChemComm

Accepted Manuscript

This article can be cited before page numbers have been issued, to do this please use: Y. H. E. Mohammed and S. Ara Khanum, *Med. Chem. Commun.*, 2018, DOI: 10.1039/C7MD00593H.

ROYAL SOCIETY OF CHEMISTRY

rsc.li/medchemcomm

View Article Online
DOI: 10.1039/C7MD00593H

The critical role of novel benzophenone analogs on tumor growth inhibition targeting angiogenesis and apoptosis

Yasser Hussein Eissa Mohammed[1,2] and Shaukath Ara Khanum[1*].

[1]*Department of Chemistry, Yuvaraja's College, University of Mysore, Mysore- 570005 Karnataka, India.*

[2]*Department of Biochemistry, Faculty of Applied Science College, University of Hajjah, Yemen.*

[*]Correspondence Author:
Dr. Shaukath Ara Khanum
Associate Professor and Head
Department of Chemistry,
Yuvaraja's College,
University of Mysore, Mysuru.
Phone: +91 - 99018 88755
Fax: +821- 2419239
Email: shaukathara@yahoo.co.in

View Article Online
DOI: 10.1039/C7MD00593H

ABSTRACT

In modern biology, one of the major importance is the progress of anti-cancer drugs with specific targets. The angiopreventive and *in vitro* tumor inhibition activities of novel synthetic benzophenone analogs were given more attention and explored in a very professional way. The multistep synthesis of novel benzophenone analogs (**9a-d** and **10a-d**) allowing substitution with methyl, choloro and flouro groups at different positions on the identical chemical backbone and the variations in the number of substituents were synthesized and characterized. In this study, we further evaluated the newly synthesized compounds for cytotoxic and anti-proliferative effects against the A549, HeLa and MCF-7 cells. For anti-angiogenic effects, further assessments were made for the potent lead compound. Through structure activity relationship, we found that an increase in the number of methyl, chloro and fluoro groups in a ring of benzophenone on compound **9d** resulted in higher potency compared to other compounds. The tumor inhibition was importantly suppressed and reflected by the neovessel formation in *in vivo* systems, such as the CAM. Compound **9d** interacts with rVEGF by hydrogen bond in-silico, thereby down regulates the VEGF expression in angiogenesis. Through the investigation, it is suggested that the compound **9d** on clonogenesis and cell migration assays have the potency to exhibit the prolonged activity with cell cycle arrest on G2/M phase against cancer progression. In addition to that, through caspase activated DNase mediated apoptosis the compound **9d** inhibit A549 cells.

Keywords: Benzophenone; MCF-7; A549; VEGF; Docking.

View Article Online
DOI: 10.1039/C7MD00593H

1. Introduction

Angiogenesis, which are considered as one of the most crucial processes in tumor progression, are known as the development of new blood vessels from the earlier vasculature. Angiogenesis word which can set up its own particular blood supply is called tumor growth [1]. The activity of many proangiogenic factors that include Vascular endothelial growth factor (VEGF), fibroblast growth factor 1 and 2, tumor necrosis factor alpha, angiogenin, tumor growth factor beta, platelet-derived growth factor, angiopoietin and pleiotrophin of the few elements portrayed, intercedes the enlistment of new blood vessel growth by a tumor [2,3]. The vascular endothelial growth factor (VEGF) is one of the most important motivating factor in charge of liquid gathering in the ovarian hyper incitement syndrome. It can be found in different tissues including edema arrangement in the cerebrum, synovial fluid and malignant ascites [4]. In most human diseases, the major part of the tumor cells mystery VEGF [5] and VEGF mRNA is severely upregulated [6]. Prolonged intratumoral miniaturized scale vessel thickness in breast cancer patients is strongly linked up with VEGF expression [7]. It has been obviously defined that angiogenesis are vital for a tumor to end up prominently expansive and dangerous. A new healing window to growth treatment may be given when there is an interference of the procedure of angiogenesis either by concealment of angiogenic progress factors. The ability to increase, as well as to down regulate cell passing and generate angiogenesis are mainly considered as major requirements for creating tumor neovasculature. Consequently, researchers have paid more attention and focused deeply in the study of the expansion of anti-angiogenesis and apoptosis as one of the most dominant concentrations in current tumor treatment. The improvement of such novel, powerful and less or no toxic compounds with different methods of activity for the

View Article Online
DOI: 10.1039/C7MD00593H

focused growth treatment leads to the existence of a creative method and efforts which are directed toward finding such anti-cancer agents [8-10].Created by both natural and synthetic ways, benzophenones are the class of pharmacologically active molecules. Different analogues of benzophenones which are featured by their high activity as anti-tumor and anti-angiogenic possibilities have been found and they are under clinical trials. Benzophenone moiety alone is not that much potentially active as anti-tumor in comparison to benzophenone integrated with heterocyclic analogues. In this unique circumstance, to get a potential approach towards the disclosure of anti-angiogenic drug the benzophenones are amalgamated with another arrangement of synthetic gatherings which have a vital part in the field of medicinal chemistry. Subsequently, it is extremely fundamental to incorporate and create novel benzophenone analogues with different targets [11, 12]. Several assessments have been made during this study for the purpose of studying the anti-angiogenic and proapoptotic and some benzophenone analogues have also been synthesized.

2. Results and discussion

2.1. Chemistry

Synthesis of the target compounds **2**-(4-benzoylphenoxy)aceto-N(N-methyl imidazole)carbonyl hydrazides **9a-d** and 2-(4-benzoylphenoxy)aceto-N(pyrone -2-one)carbonyl hydrazides **10a-d** were performed according to the reactions illustrated in scheme 1. The key starting compounds, phenyl benzoates **3a-d**, were prepared according to the published procedures [11], starting from the commercially available substituted phenols **1a-b** with substituted benzoyl chlorides **2a-d**. Fries rearrangement of compounds **3a-d** with anhydrous aluminum chloride as a catalyst gave hydroxybenzophenones **4a-d**. Furthermore, etherification of **4a-d** with chloro ethyl acetate afforded the substituted ethyl esters **5a-d**, which were

View Article Online
DOI: 10.1039/C7MD00593H

converted to the corresponding acetohydrazides **6a-d** upon treatment with hydrazine hydrate. The corresponding final compounds **9a-d** and **10a-d** were successfully synthesized by coupling compounds **6a-d** with N-methyl imidazole-4-carboxylic acid (**7)** and 2-oxo-2H-pyrone -5-carboxylic acid (**8)** respectively using TBTU as a coupling reagent and lutidine as a base. All the structures of newly synthesized compounds were assigned on the basis of their spectroscopic data such as, IR, NMR, LC-MS and also by C, H, N analysis. The compounds **3a-d**, **4a-d** and **5a-d** were synthesized and characterized earlier by our research group [15]. The spectra of the compound **6a** was considered as a representative example of the series **6a-d**. In IR spectrum, the compound **6a** showed bands at 1610, 1645 and 3100-3205 cm^{-1} corresponding to aromatic carbonyl, amide carbonyl and NH-NH_2 stretching frequencies respectively. In ^1H NMR spectrum compound **6a** showed three singlets for NH_2, OCH_2 and NH at δ 4.35, δ 4.89 and δ 9.02 respectively and also showed multiplet signals in the range δ 7.01-8.86 for aromatic protons. The mass spectra of compound **6a** gave significant stable M+1 peak at m/z 270. The IR spectra of compounds **9a** and **10a** has shown new absorption bands for amide 1735 cm^{-1} and 1725 cm^{-1} respectively compared to compound **6a** also shown disappearance of the NH_2 protons peak of the compound **6a**. In addition, ^1H NMR spectra of compounds **9d** and **10a** showed disappearance of NH_2 protons peak at 4.35 and appearance of new NH proton peak at δ 10.39 and 10.34 respectively. Also, there is an increase in aromatic protons in compounds **9d** andn**10a** as compared with compound **6a** which revealed the formation of the title compounds **9a** and **10a**. The mass spectra of compounds **9a** gave significant stable peak at m/z 379 (M+1) and **10a** at m/z 392 (M+). Further, all the target compounds **9a-d** and **10a-d** were clearly confirmed by ^{13}C NMR spectroscopy.

2.2. Biology

View Article Online
DOI: 10.1039/C7MD00593H

2.2.1. Evaluation of IC_{50} values and *in vitro* selection of lead compound

The benzophenone derivatives are known to be pharmacologically effective molecules against various pathological conditions including cancer. Earlier, our group has reported synthesis of benzophenones conjugated with thiazole, benzimidazole, coumarin and oxadiazole moieties having an anti-tumor, anti-angiogenic and proapoptotic properties against various cell lines [11, 14, 15-18].]. On the other hand, as per the literature survey imidazole and pyrone nucleus derivatives have excellent pharmacological characteristics against the variety of pathological conditions including cancer of the different cells. In the present investigation, new potent analogues were synthesized, by integrating imidazole and pyrone nucleus to benzophenone moiety. Initially, anti-proliferative efficacy of benzophenone analogues **9a-d** and **10a-d** bearing imidazole and pyrone nucleus were evaluated against human cancer cells such as, human lung adenocarcinoma (A549), human cervical adenocarcinoma (HeLa), human breast adenocarcinoma (MCF-7) and normal fibroblast cells (NIH-3T3) by performing trypan blue, 3-(4,5-dimethylthiazol-2-yl)-2,5-diphenyltetrazolium bromide (MTT) and , lactate dehydrogenase (LDH) leak assays [table 1.1]. In this series, compound **9d** was found to exhibit a promising anti-neoplastic effect in trypan blue and MTT assay with half maximal inhibitory concentration IC_{50} values as 9.6±1.7, and 8.8±0.12 μM, in A549 cells, 10.2±0.3 and 9.9±1.5 μM in Hela cells and 9.5±0.7 and 9.8±1.0 μM in MCF-7 cells respectively. Remarkably compound **9d** exhibited very negligible toxicity 94.2±1.7 μM to NIH-3T3 cells. The evaluation of cellular integrity using an LDH release assay is one of the incomparable methods to assess the cytotoxic effect of compounds. In our investigation the results shown concentration dependent increase in the release of LDH as the cells lose their integrity upon treatment with compound **9d** with IC_{50} values as 9.1±0.5, 10.4±2.1 and 9.4±0.9 μM in A549, HeLa and MCF-7 cell lines respectively.

View Article Online
DOI: 10.1039/C7MD00593H

Altogether these results suggest that, the compound **9d** was potent and prone to exhibit a cytotoxic effect against the cells of different origin. The effect of compound **9d** could be due to the presence of methyl, chloro and fluoro groups at benzophenone moiety and also due to methyl group at imidazole ring, which is unique from other compounds of the same series [figure 2]. Hence the compound **9d** was chosen as a lead compound and investigated further for its *in vitro* and *in silico* activities.

2.2.2. Structure activity relationship (SAR).

The compounds which contain the benzophenone pharmacophores are known to be pharmacologically active molecules which are utilized against several pathological conditions including cancer [16, 19, 20]. The multistep synthesis of benzophenone containing imidazole and pyrone analogues is involved in our current study. It is apparent that the compound **9d** containing the same backbone structure of benzophenone with aceto moiety and N-methyl imidazole ring as in the same series but with methyl group in the benzophenone moiety has shown good activity compared same series. The IC_{50} values as shown in table 1 suggested that the compound **9d** with a methyl, chloro and fluoro groups at benzophenone moiety and another methyl group at imidazole ring shown average IC_{50} value as ~9.6 μM as verified by trypan blue, MTT and LDH release assay. The results illustrated that, the compounds **9a** without halo groups, **9b** and **9c** with chloro and fluoro groups shown decreased activity as compared to **9d** [table 1]. It reveals that the compound **9d** with a methyl, chloro and fluoro groups in benzophenone moiety and a methyl group in the imidazole ring [figure.2.] is an important compound for biological activity. While other compounds with different substituents has shown poor cytotoxicity [table 1]. Therefore compound **9d** was selected as a lead compound based on its significant structure activity

View Article Online
DOI: 10.1039/C7MD00593H

relationship compared with other analogues and further evaluated by *in vitro, in vivo* and *in silico* studies.

2.2.3. Compound 9d exhibit the prolonged anti-mitogenicity activity.

The colony formation assay is an appropriate method to investigate the long term anti-mitogenicity of cytotoxic molecules in cancer cell proliferation. The reticence in colony formation considers as a prolonged cytotoxic effect of the active biomolecule [13]. In this analysis, A549 cells was treated with or without compound **9d** for analyzing long term effect. Results revealed that the compound **9d** visibly diminished the clonogenic efficiency of A549 cells. Compound **9d** were found to inhibit the colony formation of A549 cells by 25 and 50 µM compared to the standard cisplatin [figure 5.3. a and c], and density of the colony formation is remarkably reduced by compound **9d** which is apparent from microscopic analysis of the colonies [figure 5.3 b].

2.2.4. Counteracts the cancer cell migration by compound 9d.

Most of the cancers, including lung, liver, renal, cervical breast cancer, etc., are extremely metastatic with increased migration and invasive characteristics [13, 21]. To understand the role of compound **9d** in migration, we performed scratch wound assay with A549 cells which is highly *in vitro* migratory. Cell migration into the wound was quantified by taking snapshot pictures with a regular inverted microscope at 0 and 48 h post scratch. The A549 cells migrated over a period of 48 h to fill the wound, however, compound **9d** treated cells failed to migrate into the wound and depicted a 78.83 % and 15.59 % at 50 µM and 25 µM respectively [figure 5.4. a-d]. Therefore, compound **9d** has the potency to counteract the angiogenesis and metastasis by targeting cancer cell migration.

View Article Online
DOI: 10.1039/C7MD00593H

2.2.5. Compound 9d potentially inhibits the neovascularization in non-tumor model systems.

To investigate the anti-angiogenic activity, compound **9d** was tested in different angiogenesis models induced by $rVEGF_{165}$. Based on SAR, the compound **9d** with chloro, flouro and methyl groups in benzophenone moiety and methyl group in imidazole moiety was shown highest IC_{50} value in all assay by *in vitro* studies which lead us to select compound *9d* for *in vivo* studies in which it was showed effect on VEGFr in different chorioallontoic membrane (CAM) assays. Also, decreased in the VEGF protein levels most effectively as measured by the decreased of blood vessels in CAM. The total sprouting vessels was quantified by considering $rVEGF_{165}$ induced control as 100 % in *in vivo* CAM and *ex vivo* CAM [2, 14]. The PBS alone treated in normal developing CAM was found to be 20 % of growing blood vessels in both *in vivo*, and *ex vivo* CAM assay. A clear avascular zone around the implanted disc with compound **9d** was clearly evident for the regression of neovessels in the developing embryos in both *in vivo* and *ex vivo* CAM [figure.5. a and b] with the inhibition of 24 and 26 % respectively. The total vessel length in compound **9d** treated eggs was drastically decreased to ~85 % compared to untreated eggs in both the assays [figure.5. d and e]. To re-evaluate the effect of compound **9d** on neovascularization on angiogenesis dependent tumor progression, CAM xenograft was performed by using A549 cells with $rVEGF_{165}$. The results show that the compound **9d** and cisplatin evidently reduced the tumor progression to 1.7 and 4.0 fold respectively. This results is based on the decrease in $rVEGF_{165}$ induced micro vessel density (MVD) / HPF of compound **9d** with 3.6 ± 1.6 (86.2 %) and cisplatin with 9.1± 2.5 (52.2 %) compared to untreated with 30.1 ± 1.5, in a concentration dependent manner [figure.5. c and f].

2.2.6. Effect of compound 9d on the morphology of A549 cells.

View Article Online
DOI: 10.1039/C7MD00593H

The inhibitory effect of compound **9d** on A549 cell growth may be due to induction of apoptosis. The A549 cells were stained with geimsa and the slides were observed under microscope. In the figure.6 dead cells were lightly stained with irregular cell membrane compared to the darkly stained and spherical live cells.

2.2.7. Induction of endonuclease upon the compound 9d treatment.

Endonucleases are essential for DNA fragmentation, which is a prominent feature of the apoptosis [3, 14]. Endonuclease assay results shown that the compound **9d** has promoted the endonuclease activation as visualized by DNA lysis zone [figure.7. a and b]. Furthermore, a molecular event of compound **9d** was analyzed by immunoblot where in it exhibited tumor inhibition [figure.7. c]. Additionally, degradation of DNA into multiple intermolecular small fragments of 180-200 base pairs is a distinct biochemical trait of apoptosis. Nuclear DNA treated with or without compound **9d** was analyzed by agarose gel electrophoresis [14]. The results confirmed the typical "ladder" formation of DNA treated with compound **9d** whereas the DNA from untreated cells did not show any changes and observed as a single band on an agarose gel. This study confirms that anti-angiogenesis effects of benzophenone analogues are mediated through apoptosis leading to DNA degradation [figure.7. d].

2.2.8. Compound 9d induce apoptosis on A549 cells.

To elucidate the possible mechanism of compound **9d** mediated tumor inhibition, the effect of compound **9d** on A549 cells was investigated. The treatment of compound **9d** to A549 cells induced a significant proportion of cells to undergo apoptosis, as determined by the flow cytometric analysis [13]. The flow cytometric analysis of the cells indicates the formation of apoptotic bodies and condensed camptothecin and control cells, upon receiving compound **9d** treatment some of the A549 cells undergo apoptosis and are detected in the sub-G_2 area [figure.8.

View Article Online
DOI: 10.1039/C7MD00593H

a and b]. Furthermore, compound **9d** promote the apoptotic cell death by caspase-3 activation. A molecular event of compound **9d** exhibited tumor regression was analyzed by immunoblot [figure 8. c]. These results suggested the broken DNA of A549 cells, resulting in tumor killing. The obvious ramification is the growth arrest of A549 cells.

2.2.9. Influence of compound 9d on the A549 cell cycle arrest.

Compound **9d** induces cell cycle arrest in A549 cells *in vitro*. Flow cytometric cell cycle analysis was performed using propidium iodide (PI) DNA staining [13] of A549 cells following 48 h of treatment with 85 μM compound **9d**. In A549 cell cycle analysis the compound **9d** showed arrest in G2/M phase at 24 h after treatment. However, at 48 h, the cells arrested in the G2/M phase underwent cell death as evidences by the increase in sub-G0 percentage [figure.9. a and b].

2.2.10. Docking of inhibitors with the active site of VEGF.

Autodock programming was applied to produce the protein-**9d** complex in order to understand the interaction between VEGF protein and ligand **9d**. It is clearly noticeable that ligand **9d** is placed in the center of the active site and by hydrogen bonding interactions it is stabilized. Together with their distances and angles, the hydrogen bonds exhibited in the VEGF-**9d** complex are documented. By taking into account the interaction energies of the **9d** with residues in the active site of the VEGF, noteworthy binding key residues in the active site of the model were determined and approved. This noticeable evidence, distinguished and it can clearly prove the relative significance of each residue in a positive restricting interaction shows the binding energy, ligand efficiency, inhibition constant, van der Waals force, hydrogen bond, desolvation energy, bonding residues score, and bond length score for the active site of VEGF-**9d** complex through a definition compare to the compound **9d** [table 2]. Likewise it is obvious

View Article Online
DOI: 10.1039/C7MD00593H

that the VEGF-**9d** complex has substantial perfect with bonding energies -7.66 kJ mol^{-1} [figure.10]. For the protein complex interaction we have to take into consideration all the important factors mentioned earlier. It was approved by the interaction analysis that ARG842, ASN923 and ASP1052, the amino acid residues of the VEGF were significantly attaching to the compound **9d** as the main providers for the inhibition interaction [figure.11.a-d]. Through the *in silico* study it was approved that ARG842, ASN923 and ASP1052 are the most preferred residues in the inhibitor binding reaction and this point was supported that the interaction energy does not include the contribution from the water or the expanded protein structure along with the list of hydrogen bond interactions between the protein and the active site. The VEGF structure was further applied for protein-ligand modeling studies. Positively connected with receptor binding, docking in VEGF protein play crucial role in sustaining a functional conformation. The planned interactions between the VEGF and the inhibitors in this study are of a great use for understanding and acquiring the possible mechanism of inhibitor binding. For the VEGF and the structure and function of biological molecules, it is apparent that hydrogen bonds have significant roles. Also, ARG842, ASN923 and ASP1052 are important for strong hydrogen bonding interaction with the inhibitors.

It is obvious that, molecule **9d**, is the most likely inhibitor and ARG842, ASN923 and ASP1052 residues are involved in inhibitor binding and forms hydrogen bonding with the inhibitors. It should be taken into consideration that ARG842, ASN923 and ASP1052 are vital for receptor binding or preserving the hydrophobicity of the inhibitor binding pocket.

3. Conclusion

Through the current study, two series of novel benzophenone analogues containing imidazole (**9a-d)** and pyrone nucleus (**10a-d**) were synthesized. It was suggested by the

View Article Online
DOI: 10.1039/C7MD00593H

structural activity relationship of these compounds that, the compound **9d** with a methyl, chloro and fluoro groups in benzophenone moiety, shown anti-angiogenesis effect against A549, HeLa and MCF-7 cell lines with IC_{50} of 9.1±0.5, 10.4±2.1 and 9.4±0.9 μM respectively and selected as the lead compound within this series. The results observed in the CAM models for the inhibition of neovascularization and tumor growth strongly supported our hypothesis. Compound **9d** interacts with rVEGF by hydrogen bond *in silico*, thereby down regulates the VEGF expression in angiogenesis. Further, the compounds **9d** have the potency to exhibit the prolonged activity with cell cycle arrest on G2/M phase against cancer progression this may be by the interaction of the compound **9d** with VEGF-A secretion as verified by cell cycle analysis study and immunoblot. Therefore, in conclusion we can state that the compound **9d** plays a crucial role as angiopreventive effect and it can be applied in various fields related to cancer therapeutics [figure.12].

4. Materials and methods

4.1. Experimental section

The chemicals required for the synthesis of the title compounds **9a-d** and **10a-d** were procured from Sigma Aldrich Chemical Co. The completion of reaction was checked by thin layer chromatography (TLC) which was performed on aluminum backed silica plates and the spots were detected by exposure to UV-lamp at λ= 254 nm. Melting points and boiling point were measured on a chemiline, microcontroller based melting point/ boiling point-Cl725 apparatus with a digital thermometer. IR spectra were recorded on the Agilent Technologies, Cary 630 FTIR spectrometer, ^{1}H and ^{13}C NMR spectra were recorded on VNMRS-400 Agilent-NMR spectrophotometer. The mass spectra were obtained with a VG70-70H spectrometer and

View Article Online
DOI: 10.1039/C7MD00593H

the elemental analysis (C, H, and N) was performed on ElementarVario EL III elemental analyzer. The results of elemental analyses are within ±0.4 % of the theoretical values.

Cell lines, like A549, HeLa, MCF-7 and normal NIH-3T3 cells were procured from NCCS, Pune, India. DMEM, sodium carbonate, fetal bovine serum (FBS), MTT from Sigma Aldrich, USA. All cell culture wares are from Eppendorf, Germany. Penicillin- Streptomycin (Sigma-Aldrich, USA). All photographs were taken using Canon power shot Sx500 IS camera.

4.2. Chemistry: Plan of the synthesis

Novel benzophenone analogues **9a-d** and **10a-d** synthesis was accomplished according to the steps illustrated in scheme1. First, substituted phenols **1a-b** on reaction with substituted benzoyl chlorides **2a-d** in the presence of trimethylamine (TEA) gave substituted phenyl benzoates **3a-d**. Compounds **3a-d** on subjection to fries rearrangement afforded substituted diaryl methanones commonly known as hydroxy benzophenones **4a-d**. Then (2-aroyl-4-methylphenoxy) acetates **5a-d** were achieved in excellent yield by reacting compounds **4a-d** with ethyl bromoacetate in the presence of anhydrous potassium carbonate and dry acetone. Further, compounds **5a-d** on treatment with 99 % hydrazine hydrate gave different hydrazides **6a-d**. Finally, compounds **6a-d** on coupling with 1-methyl-1H-imidazole-4-carboxylic acid (**7**) and separately with 2-oxo-2H-pyrone -5-carboxylic acid (**8**) in the presence of o-(benzotriazol-1-yl)-N,N,N′,N′- tetra methyl uranium tetra fluoro borate (TBTU) and lutidine as a coupling agent furnished the title compounds **9d** and **10d** in excellent yield.

4.2.1. General procedure for the synthesis of benzoic acid phenyl ester (3a-d).

Substituted phenyl benzoates **3a-d** was synthesized by dissolving substituted phenol **1a-b** and TEA (0.45 mol) in dichloro methane (DCM). Then the reaction mixture was cooled to 0 ºC.

View Article Online
DOI: 10.1039/C7MD00593H

Further, a solution of substituted benzoyl chloride **2a-d** (0.23 mol) in DCM was slowly added to the reaction mixture and stirred for 5 h and the completion of the reaction was monitored by TLC using 4:1 n-hexane: ethyl acetate solvent mixture. Then the reaction mass was diluted with DCM (100 ml) and washed with 10 % sodium hydroxide solution (3×40 ml), followed by water (3×30 ml). The organic layer was dried over anhydrous sodium sulphate and the solid obtained after evaporation of the solvent was recrystallized from ethanol to give compounds **3a-d**.

4.2.1.1. Phenyl benzoate (3a).

Yield: 86 %; M.P. 52-54 ºC; FT-IR (KBr, ν_{max} cm^{-1}): 1738 (C=O), 1130 (C-O), 722 (Ar bending); ^{1}H NMR ($DMSOd_6$): 7.12-8.41 (m, 10H, Ar-H); ^{13}C NMR (DMSO-d_6) δ: 121.73, 126.02, 128.55, 129.34, 130.41, 133.92, 149.50, 165.23; LC-MS m/z: 198 (M+) peak showed that m/z is equivalent to molecular weight. Anal. Calcd. For $C_{13}H_{10}O_2$: C, 77.93; H, 5.09. Found: C, 77.90; H, 5.04 %.

4.2.1.2. 2-Fluoro-6-chloro Phenyl-4-fluoro benzoate (3b).

Yield: 94 %; M.P. 54-56 ºC; FT-IR (KBr, ν_{max} cm^{-1}): 1740 (C=O), 1150 (C-O), 722 (Ar bending); ^{1}H NMR (DMSO-d_6) δ: 6.94-8.28 (m, 7H, Ar-H); ^{13}C NMR (DMSO-d_6) δ: 114.03, 115.46, 125.92, 127.23, 128.55, 129.34, 131.41, 132.02, 140.53, 161.03, 165.31, 16817; LC-MS m/z 268 (M+), 270 (M+2). Anal. Calcd. For $C_{13}H_7ClF_2O_2$: C, 58.12; H, 2.63. Found: C, 58.22; H, 2.43 %.

4.2.1.3. 2-Fluoro-6-chloro phenyl-4-chloro benzoate (3c).

Yield: 95 %; M.P. 55-57 ºC; FT-IR (KBr, ν_{max} cm^{-1}): 1750 (C=O), 1145 (C-O), 722 (Ar bending); ^{1}H NMR (DMSO-d_6) δ: 6.92-8.12 (m, 7H, Ar-H); ^{13}C NMR (DMSO-d_6) δ: 114.03, 127.32, 128.13, 129.15, 131.04, 131.71, 139.52, 140.53, 161.03165.23; LC-MS m/z 285 (M+),

View Article Online
DOI: 10.1039/C7MD00593H

287 (M+2), 289 (M+4). Anal. Calcd. For$C_{13}H_7Cl_2FO_2$: C, 54.77; H, 2.47. Found: C, 54.57; H, 2.33 %.

4.2.1.4. 2-Fluoro-6-chloro phenyl-4-methyl benzoate (3d).

Yield: 96 %; M.P. 62-63 ºC; FT-IR (KBr, ν_{max} cm-1): 1780 (C=O) 1138 (C-O), 722 (Ar bending); ^{1}H NMR (DMSO-d6): δ 2.3 (s, 3H, CH3), 7.38-8.07 (m, 7H, Ar-H); ^{13}C NMR (DMSO-d_6) δ: 21.34, 114.05, 127.32, 128.13, 130.24, 131.64, 140.51, 143.62, 161.03165.33; LC-MS m/z 264 (M+), 266 (M+2). Anal. Calcd. For $C_{14}H_{10}ClFO_2$: C, 63.53; H, 3.81. Found: C, 63.59; H, 3.79 %.

4.2.2. 4.2.2. General procedure for the synthesis of 4-hydroxy benzophenones (4a-d).

Substituted 4-hydroxy benzophenones **4a-d** were synthesized by Fries rearrangement. Compounds **3a-d** (0.065 mol) were blended with aluminium chloride (0.128 mol) and the mixture was heated to 150 ºC this temperature was maintained for 3 h and the completion of the reaction was monitored by TLC using 4:1 n-hexane: ethyl acetate solvent mixture. Then the reaction mixture was cooled to room temperature and quenched with 7 N hydrochloric acid and ice water. The reaction mixture was stirred for about 2 h, the solid obtained was filtered and recrystallized with methanol to obtain desired compounds **4a-d**.

4.2.2.1. (4-Hydroxyphenyl)(phenyl)methanone (4a).

Yield: 61 %; M.P. 146-147 ºC; FT-IR (KBr, ν_{max} cm^{-1}): 1671 (C=O), 3545-3635 (O-H); ^{1}H NMR (DMSO-d_6) δ: 6.81-7.81 (m, 9H, Ar-H), 9.68 (s, 1H, OH); ^{13}C NMR (DMSO-d_6) δ: 116.11, 128.42, 130.01, 130.02, 131.43, 131.74, 132.51, 138.41, 162.03, 194.53; LC-MS m/z 198 (M+). Anal. Calcd. For $C_{13}H_{10}O_2$: C, 78.72; H, 5.08. Found: C, 78.69; H, 5.06 %.

4.2.2.2. (3-Chloro-5-fluoro-4-hydroxyphenyl)(4-fluorophenyl)methanone (4b).

View Article Online
DOI: 10.1039/C7MD00593H

Yield: 61 %; M.P. 148-149 ºC; FT-IR (KBr, ν_{max} cm^{-1}): 1671 (C=O), 3545-3635 (-OH); ^{1}H NMR (DMSO-d_6) δ: 7.36-7.82 (m, 6H, Ar-H), 11.64 (bs, 1H, OH); ^{13}C NMR (DMSO-d_6) δ: 114.21, 115.23, 125.42, 127.31, 130.32, 131.43, 134.04, 135.51, 148.41, 154.81, 166.03, 194.33; LC-MS m/z 268 (M+) and 270 (M+2). Anal. Calcd. For $C_{13}H_7ClF_2O_2$: C, 58.12; H, 2.63. Found: C, 58.21; H, 2.52 %.

4.2.2.3. (3-Chloro-5-fluoro-4-hydroxyphenyl)(4-chlorophenyl)methanone (4c).

Yield: 68 %; M.P. 167-169 ºC; FT-IR (KBr, ν_{max} cm^{-1}): 1660 (C=O), 3525-3625 (-OH);^{1}H NMR (DMSO-d_6) δ: 7.12-7.74 (m, 6H, Ar-H), 11.60 (s, 1H, OH);); ^{13}C NMR (DMSO-d_6) δ: 114.21, 125.42, 127.41, 128.62, 131.72, 135.33, 136.54, 138.01, 148.41, 154.81, 166.03, 194.33; LC-MS m/z 285 (M+), 287 (M+2) and 289 (M+4). Anal. Calcd. For $C_{13}H_7Cl_2FO_2$: C, 54.77; H, 2.47. Found: C, 54.65; H, 2.32 %.

4.2.2.4. (3-Chloro-5-fluoro-4-hydroxyphenyl)(4-methylphenyl)methanone (4d).

Yield: 65 %; M.P. 182-183 ºC; FT-IR (KBr, ν_{max} cm^{-1}): 1635 (C=O), 3430-3590 (OH); ^{1}H NMR (DMSO-d6) δ: 2.73 (s, 3H, CH_3), 7.15-7.68 (m, 6H, Ar-H), 9.46 (s, 1H, OH);); ^{13}C NMR (DMSO-d_6) δ: 21.13, 114.21, 125.52, 127.41, 128.62, 130.32, 142.23, 148.41, 154.81, 194.33; LC-MS m/z 265 (M+) and 267 (M+2). Anal. Calcd. For $C_{14}H_{10}ClFO_2$: C, 63.53; H, 3.81; Cl, 13.39; F, 7.18. Found: C, 63.55; H, 3.83; Cl, 13.41; F, 7.21 %.

4.2.3. General procedure for the synthesis of (4-benzoyl-phenoxy)- acetic acid ethyl esters (5a-d).

To a solution of compounds **4a-d** (0.036 mol) in dry acetone (70 ml), potassium carbonate (0.078 mol) and ethyl bromoroacetate (0.057 mol) were added and the reaction mass was heated to 60 ºC for 4-6 h, The progress of the reactions was monitored by TLC using 2:1 n-

View Article Online
DOI: 10.1039/C7MD00593H

hexane: ethyl acetate solvent mixture. The reaction mixture was cooled and the solvent was removed by distillation. The residual mass was triturated with cold water to remove potassium carbonate, and extracted with ether (3 × 50 ml). The ether layer was washed with 10 % sodium hydroxide solution (3 × 50 ml) followed by water (3 × 30 ml), dried over anhydrous sodium sulphate and evaporated to dryness to obtain crude solid, which, on recrystallization with ethanol afforded desired compounds **5a-d**.

4.2.3.1. (4-Benzoylphenoxy)acetic acid ethyl ester (5a).

Yield: 90 %; M.P. 47-49 ºC; FT-IR (KBr, ν_{max} cm^{-1}): 1660 (C=O), 1730 (ester, C=O), 1130 (C-O); ^{1}H NMR (DMSO-d_6) δ: 1.28 (t, 3H, CH_3 of ester), 4.21 (q, *J*=6 Hz, 2H, CH_2 of ester), 5.03 (s, 2H, CH_2), 6.92 -7.83 (m, 9H, Ar-H); ^{13}C NMR (DMSO-d_6) δ: 61.33, 65.31, 114.03, 128.43, 130.02, 130.72.41, 131.37, 138.52, 161.93, 169.41, 194.43; LC-MS: m/z: 285 (M+). Anal. Calcd. For $C_{17}H_{16}O_4$: C, 71.82; H, 5.67. Found**:** C, 71.85; H, 5.69 %.

4.2.3.2. (4-Fluorobenzoyl-2-chloro-6-fluorophenoxy)acetic acid ethyl ester (5b).

Yield: 85 %; M.P. 50-52 ºC; FT-IR (KBr, ν_{max} cm^{-1}): 1660 (C=O), 1730 (ester, C=O), 1135 (C-O); ^{1}H NMR (DMSO-d_6) δ: 1.27 (t, 3H, CH_3 of ester), 4.21 (q, *J*=6 Hz, 2H, CH_2 of ester), 5.03 (s, 2H, CH_2), 7.58-7.77 (m, 6H, Ar-H); ^{13}C NMR (DMSO-d_6) δ: 61.33, 64.95, 114.03, 115.24, 123.94, 126.93, 133.52, 134.12.41, 135.37, 153.52, 166.93, 169.41, 194.43; LC-MS: m/z: 354 (M+) and 356 (M+2). Anal. Calcd. For $C_{17}H_{13}ClF_2O_4$: C, 57.56; H, 3.69. Found: C, 57.41; H, 3.52 %

4.2.3.3. [2-Chloro-4-(4-chloro-benzoyl)-6-fluoro-phenoxy]-acetic acid ethyl ester (5c).

Yield: 83 %; M.P. 54-56 ºC; FT-IR (KBr, ν_{max} cm^{-1}): 1650 (C=O), 1740 (ester, C=O), 1135 (C-O); ^{1}H NMR (DMSO-d_6) δ: 1.27 (t, *J*=7 Hz, 3H, CH_3 of ester), 4.12 (q, *J*=6 Hz, 2H, CH_2 of

View Article Online
DOI: 10.1039/C7MD00593H

ester), 4.92 (s, 2H, CH_2), 7.59-7.75 (m, 6H, Ar-H); ^{13}C NMR (DMSO-d_6) δ: 61.33, 64.95, 114.03, 115.24, 123.94, 126.93, 133.52, 134.12.41, 135.37, 153.52, 166.93, 169.41, 194.43; LC-MS: m/z: 371 (M+), 373 (M+2) and 375 (M+4). Anal. Calcd. For $C_{17}H_{13}Cl_2FO_4$: C, 55.01; H, 3.53. Found: C, 55.19; H, 3.41 %.

4.2.3.4. (4-Methylbenzoyl-2-chloro-6-fluorophenoxy)acetic acid ethyl ester (5d).

Yield: 83 %; M.P. 62-63 ºC;FT-IR (KBr, ν_{max} cm^{-1}): 1650 (C=O), 1740 (ester, C=O), 1125 (C-O); ^{1}H NMR (DMSO-d_6) δ: 1.25 (t, *J*=7 Hz, 3H, CH_3 of ester), 2.32 (s, 3H, CH_3), 4.19 (q, *J*=6 Hz, 2H, CH_2 of ester) 5.02 (s, 2H, CH_2), 7.24-7.66 (m, 6H, Ar-H); ^{13}C NMR (DMSO-d_6) δ: 21.31, 61.33, 64.95, 114.03, 123.94, 126.21, 127.75, 130.25, 135.37, 142.11, 153.32, 169.41, 194.43; LC-MS: m/z: 351 (M+), 352 (M+2). Anal. Calcd. For $C_{18}H_{16}ClFO_4$: C, 61.64; H, 4.60; Cl, 10.11; F, 5.42. Found: C, 61.66; H, 4.63; Cl, 10.13; F, 5.44 %.

4.2.4. General procedure for the synthesis of 2-(4-benzoyl-phenoxy)acetohydrazides (6a-d).

Hydrazine hydrate (0.018 mol) was added to a solution of compounds **5a-d** (0.018 mol) in ethanol (30 ml) and continuously stirred for 3 h at room temperature. The completion of the reaction was monitored by TLC using 2:1 chloroform: ethyl acetate as a mobile phase. After the separation of a white solid, it was quenched with water (50 ml), filtered and washed with water (50 ml). The solid was dried under vacuum and the product was recrystallized from ethanol to obtain compounds **6a-d** in good yield.

4.2.4.1. 2-(4-Benzoylphenoxy)acetohydrazide (6a).

Yield: 76 %; M.P. 107-109 ºC; FT-IR (KBr, ν_{max} cm^{-1}): 1610 (C=O), 1645 (amide, C=O), 3100-3205 (NH-NH_2); ^{1}H NMR (DMSO-d_6) δ: 4.35 (s, 2H, NH_2), 4.89 (s, 2H, OCH_2), 7.01-8.86 (m, 9H, Ar-H), 9.02 (s, 1H, NH); ^{13}C NMR (DMSO-d_6) δ: 66.25, 114.11, 128.44, 130.21,

View Article Online
DOI: 10.1039/C7MD00593H

131.05, 132.45, 138.37, 161.41, 166.31, 194.43; LC-MS m/z 270 (M+). Anal. Calcd. For $C_{15}H_{14}N_2O_3$: C, 66.66; H, 5.22; N, 10.36. Found: C, 66.68; H, 5.24; N, 8.13 %.

4.2.4.2. [2-4(4-Fluoro)benzoyl-2-chloro-6-fluorophenoxy]aceto hydrazide (6b).

Yield: 79 %; M.P. 110-113 ºC; FT-IR (KBr, ν_{max} cm^{-1}): 1620 (C=O), 1645 (amide, C=O), 3100-3205 (NH-NH_2); ^{1}H NMR (DMSO-d_6) δ: 4.35 (s, 2H, NH_2), 4.69 (s, 2H, OCH_2), 7.20-7.86 (m, 6H, Ar-H), 9.32 (s, 1H, NH); ^{13}C NMR (DMSO-d_6) δ: 65.95, 114.31, 123.85, 126.93, 133.45, 134.01, 135.04, 153.41, 166.61, 194.43; LC-MS m/z: 340 (M+) and 342 (M+2). Anal. Calcd. For $C_{15}H_{11}ClF_2N_2O_3$: C, 52.88; H, 3.25; Cl, 10.41; F, 11.15; N, 8.22. Found: C, 52.75; H, 3.38 %.

4.2.4.3. 2-(2-Chloro-4-(4-chlorobenzoyl)-6-fluorophenoxy)acetohydrazide (6c).

Yield: 79 %; M.P. 112-116 ºC; FT-IR (KBr, ν_{max} cm^{-1}): 1610 (C=O), 1645 (amide, C=O), 3100-3205 (NH-NH_2); ^{1}H NMR (DMSO-d_6) δ: 4.35 (s, 2H, NH_2), 4.83 (s, 2H, OCH_2), 7.20-7.76 (m, 6H, Ar-H), 9.32 (s, 1H, NH); ^{13}C NMR (DMSO-d_6) δ: 65.95, 114.31, 115.22, 123.85, 126.93, 133.45, 134.01, 135.04, 153.41, 166.61, 194.43; LC-MS m/z 357 (M+) and 359 (M+2). Anal. Calcd. For $C_{15}H_{11}Cl_2FN_2O_3$: C, 50.44; H, 3.10; Cl, 19.85; F, 5.32; N, 7.84. Found: C, 50.46; H, 3.13 %.

4.2.4.4. [2--4(4-Methyl)benzoyl-2-chloro-6-fluorophenoxy]aceto hydrazide (6d).

Yield: 79 %; M.P. 117-123 ºC; FT-IR (KBr, ν_{max} cm^{-1}): 1610 (C=O), 1645 (amide, C=O), 3100-3205 (NH-NH_2); ^{1}H NMR (DMSO-d_6) δ: 2.40 (s, 2H, CH_3), 4.31 (s, 2H, NH_2), 4.79 (s, 2H, OCH_2), 7.20-7.86 (m, 6H, Ar-H), 9.32 (s, 1H, NH);); ^{13}C NMR (DMSO-d_6) δ: 21.34, 65.95, 114.31, 123.85, 126.93, 128.73, 130.22, 135.45, 142.21.04, 153.31, 166.61, 194.43; LC–MS m/z

View Article Online
DOI: 10.1039/C7MD00593H

336 (M+) and 338 (M+2). Anal. Calcd. For $C_{16}H_{14}ClFN_2O_3$: C, 57.07; H, 4.19; Cl, 10.53; F, 5.64; N, 8.32. Found: C, 57.09; H, 4.22 %.

4.2.5. General procedure for the synthesis of 2-(4-benzoylphenoxy)aceto-*N* (*N*-methyl imidazole)carbonyl hydrazides (9a-d).

2-(4-Benzoylphenoxy)acetohydrazides **6a-d** (0.0010 mol) in dry DCM (20 ml) was stirred at 25-30 ºC, and then lutidine (0.0015 mol) was added, followed by the addition of N-methyl imidazole-4-carboxylic acid (**7**, 0.0010 mol). The reaction mixture was stirred at the same temperature for 30 minutes, then cooled to 0-5 ºC and TBTU (0.0015 mol) was added and the temperature was maintained to 5 ºC over a period of 30 minutes. The reaction mass was stirred overnight and monitored by TLC using chloroform: methanol (9:1) as the mobile phase. Then the solvent was evaporated at reduced pressure, quenched by the addition of crushed ice and the solid obtained was filtered, dried and recrystallized from ethanol to afford compounds **9a-d** in good yield.

4.2.5.1. 2-(4-benzoylphenoxy)aceto-*N*(*N*-methyl imidazole)carbonyl hydrazide (9a).

Yield: 93 %; Purity > 96 % HPLC; M.P. 103-105 ºC; FT-IR (KBr, ν_{max} cm^{-1}):1650 (C=O), 1678 (-CH_2-C=O), 1735 (C=O), 3275-3360 (NH-NH); ^{1}H NMR (DMSO-d_6) δ: 3.71 (s, 3H, CH_3), 4.86 (s, 2H, OCH_2), 6.91-8.08 (m, 11H, Ar-H), 9.89 (s,1H, NH), 10.39 (s, 1H, NH), ; ^{13}C NMR (DMSO-d_6) δ: 32.16, 72.77, 114.09,123.03, 126.04, 128.73, 130.11, 130.59, 131.65, 132.18, 137.80, 140.21, 165.70, 167.34, 175.45, 187.38; LC-MS m/z 379 (M+1) and 380 (M+2). Anal. Calcd. For $C_{20}H_{18}N_4O_4$: C, 63.48; H, 4.79; N, 14.81, Found: C, 63.46; H, 4.78; N, 14.82 %.

View Article Online
DOI: 10.1039/C7MD00593H

4.2.5.2. [2-4(4-Fluoro) benzoyl-2-chloro-6-fluorophenoxy]aceto-*N* (*N*-methyl imidazole) carbonyl hydrazide (9b).

Yield: 96 %; Purity > 87 % HPLC; M.P. 107-109 ºC; FT-IR (KBr, ν_{max} cm^{-1}): 1675 (C=O), 1676 (-CH_2-C=O), 1755 (C=O), 3275-3360 (NH-NH); ^{1}H NMR (DMSO-d_6) δ: 3.71 (s, 3H, CH_3), 4.86 (s, 2H, OCH_2), 6.91-8.05 (m, 8H, Ar-H), 9.87 (s, 1H, NH), 10.89 (s, 1H, NH); ^{13}C NMR (DMSO-d_6) δ: 29.16, 77.07,115.21, 116.03, 120.66,120.72, 123.00, 126.46, 127.54, 131.29, 133.65, 133.18, 140.03, 148.44, 155.51, 168.41, 167.04, 173.95, 189.78; LC-MS m/z 448 (M+) and 450 (M+2). Anal. Calcd. For $C_{20}H_{15}ClF_2N_4O_4$: C, 53.52; H, 3.37; Cl, 7.90; F, 8.47; N, 12.48, Found: C, 53.54; H, 3.35; N, 12.46 %.

4.2.5.3. [2-4(4-Chloro) benzoyl-2-chloro-6-fluorophenoxy]aceto-*N* (*N*-methyl imidazole) carbonyl hydrazide (9c).

Yield: 85 %; Purity > 85 % HPLC; M.P. 106-108 ºC; FT-IR (KBr, ν_{max} cm^{-1}): 1680 (C=O), 1679 (-CH_2-C=O), 1730 (C=O), 3275-3360 (NH-NH); ^{1}H NMR (DMSO-d_6) δ: 3.69 (s, 3H, CH_3), 4.86 (s, 2H, OCH_2), 6.91-7.85 (m, 8H, Ar-H), 9.88 (s, 1H, NH), 10.89 (s, 1H, NH); ^{13}C NMR (DMSO-d_6) δ: 28.16, 77.27, 116.79, 120.7, 123.66, 126.54, 128.51, 131.29, 133.65, 136.21, 137.50, 140.18, 148.44, 153.41, 167.01, 175.45, 194.78; LC-MS m/z 464 (M+) and 466 (M+2). Anal. Calcd. For $C_{20}H_{15}Cl_2FN_4O_4$: C, 51.63; H, 3.25; Cl, 15.24; F, 4.08; N, 12.04, Found: C, 51.62; H, 3.24; N, 12.02 %.

4.2.5.4. [2--4(4-Methyl) benzoyl-2-chloro-6-fluorophenoxy]aceto-*N* (*N*-methyl imidazole) carbonyl hydrazide (9d).

View Article Online
DOI: 10.1039/C7MD00593H

Yield: 89 %; Purity > 85% HPLC; M.P. 114-117 ºC; FT-IR (KBr, ν_{max} cm^{-1}): 1645 (C=O), 1682 (-CH_2-C=O), 1740 (C=O), 3275-3360 (NH-NH); ^{1}H NMR (DMSO-d_6) δ: 2.41 (s, 3H, Ar-CH_3), 3.71 (s, 3H, CH_3), 4.86 (s, 2H, OCH_2), 6.91-7.85 (m, 8H, Ar-H), 9.89 (1H, NH), 10.89 (s, 1H, NH); ^{13}C NMR (DMSO-d_6) δ: 26.55, 25.55, 77.93, 116.26, 120.08, 123.84, 126.61, 127.13, 128.35, 130.00, 133.12, 134.82, 141.43, 148.81, 153.13, 167.02, 170.22, 187.01; LC-MS m/z 444 (M+) and 446 (M+2). Anal. Calcd. For $C_{21}H_{18}ClFN_4O_4$: C, 56.70; H, 4.08; Cl, 7.97; F, 4.27; N, 12.59, Found: C, 56.68; H, 4.07; N, 12.58 %.

4.2.6. General procedure for the synthesis of 2-(4-benzoylphenoxy)aceto-*N*(pyrone -2-one)carbonyl hydrazides (10a-d).

Compounds **6a-d** (0.0010 mol) in dry DCM (20 ml) was stirred at 25-30 ºC, and then lutidine (0.0015 mol) was added dropwise, followed by the addition of 2-oxo-2H-pyrone -5-carboxylic acid (**8**, 0.0010 mol). The reaction mixture was stirred at the same temperature for 30 minutes, then cooled to 0-5 ºC and TBTU (0.0015 mol) was added by maintaining the temperature below 5 ºC over a period of 30 minutes. The reaction mass was stirred overnight and monitored by TLC using chloroform: methanol (9:1) as the mobile phase. The solvent was evaporated at reduced pressure, quenched by the addition of crushed ice and the obtained solid was filtered, dried and recrystallized from ethanol to afford compounds **10a-d** in good yield.

4.2.6.1. 2-(4-Benzoylphenoxy)aceto-*N*(pyrone -2-one)carbonyl hydrazide (10a).

Yield: 81 %; Purity > 85% HPLC;M.P. 112-115 ºC; FT-IR (KBr, ν_{max} cm^{-1}):1650 (C=O), 1678 (-CH_2-C=O), 1725 (C=O of pyrone e), 3275-3360 (NH-NH); ^{1}H NMR (DMSO-d_6) δ: 4.86 (s, 2H, OCH_2), 6.31-8.65 (m, 12H, Ar-H), 9.79 (s, 1H, NH), 10.34 (s, 1H, NH); ^{13}C NMR (DMSO-d_6) δ: 78.47, 105.29, 113.76, 120.93, 128.26, 130.10, 130.19, 131.20, 131.45, 138.48,

View Article Online
DOI: 10.1039/C7MD00593H

146.21, 165.71, 161.83, 165.98, 170.45, 187.38; LC-MS m/z 392 (M+). Anal. Calcd. For $C_{21}H_{16}N_2O_6$: C, 64.28; H, 4.11; N, 7.14, Found: C, 64.26; H, 4.09; N, 7.12 %.

4.2.6.2. [2--4(4-Fluoro) benzoyl-2-chloro-6-fluorophenoxy]aceto-*N*(pyrone -2-one)carbonyl hydrazide (10b).

Yield: 72 %; Purity > 81% HPLC; M.P. 116-119 ºC; FT-IR (KBr, ν_{max} cm^{-1}):1660 (C=O), 1682 (amide, C=O), 1732 (C=O of pyrone e), 3275-3360 (NH-NH); ^{1}H NMR (DMSO-d_6) δ: 4.86 (s, 2H, OCH_2), 6.31-8.65 (m, 9H, Ar-H), 9.69 (s, 1H, NH) 10.24 (s. 1H, NH); ^{13}C NMR (DMSO-d_6) δ: 77.95, 106.73, 115.21, 116.29, 120.76, 120.91, 126.91, 131.20, 131.72, 133.11, 133.37, 146.51, 148.21, 153.12, 161.03, 165.81, 165.93, 170.38, 187.42; LC-MS m/z 462 (M+) and 464 (M+2). Anal. Calcd. For $C_{21}H_{13}ClF_2N_2O_6$: C, 54.50; H, 2.83; N, 6.05, Found: C, 54.48; H, 2.81; N, 6.04 %.

4.2.6.3. [2--4(4-Chloro)benzoyl-2-chloro-6-fluorophenoxy]aceto-*N*(pyrone -2-one)carbonyl hydrazide (10c).

Yield: 67 %; Purity > 85% HPLC; M.P. 117-119 ºC; FT-IR (KBr, ν_{max} cm^{-1}): 1648 (C=O), 1679 (-CH_2-C=O), 1728 (C=O of pyrone e), 3275-3360 (NH-NH); ^{1}H NMR (DMSO-d_6) δ: 4.86 (s, 2H, OCH_2), 6.31-8.65 (m, 9H, Ar-H), 9.09 (s, 1H, NH), 10.03 (s, 1H, NH); ^{13}C NMR (DMSO-d_6) δ: 77.97, 114.21, 116.22, 120.72, 120.93, 127.12, 128.69, 131.22, 131.50, 133.11, 135.91, 137.51, 146.72, 148.82, 153.11, 161.01, 164.07, 170.32, 187.38; LC-MS m/z 478 (M+) and 450 (M+2). Anal. Calcd. For $C_{21}H_{13}Cl_2FN_2O_6$: C, 52.63; H, 2.73; N, 5.85, Found: C, 52.62; H, 2.71; N, 5.83 %.

4.2.6.4. [2-4(4-Methyl)benzoyl-2-chloro-6-fluorophenoxy]aceto-*N*(pyrone -2-one)carbonyl hydrazide (10d).

View Article Online
DOI: 10.1039/C7MD00593H

Yield: 88 %; Purity > 78 % HPLC; M.P.118-120 ºC; FT-IR (KBr, ν_{max} cm^{-1}):1650 (C=O), 1678 (-CH_2-C=O), 1728 (C=O of pyrone e), 3275-3360 (NH-NH); ^{1}H NMR (DMSO-d_6) δ: 2.40 (s, 3H, CH_3), 4.86 (s, 2H, OCH_2), 6.31-8.65 (m, 9H, Ar-H), 9.23 (s, 1H, NH), 10.23 (s, 1H, NH); ^{13}C NMR (DMSO-d_6) δ: 21.32, 77.92, 109.21, 117.22, 122.71, 126.92, 129.12, 130.69, 131.24, 131.80, 134.11, 135.81, 138.51, 146.73, 149.83, 153.18, 161.04, 164.06, 171.32, 187.58; LC-MS m/z 458 (M+) and 460 (M+2). Anal. Calcd. For $C_{22}H_{16}ClFN_2O_6$: C, 57.59; H, 3.51; N, 6.11, Found: C, 57.56; H, 3.50; N, 6.10 %.

4.3. Biological study

4.3.1. Cell culture and *in vitro* treatment.

All the experimental manipulations were carried out strictly under aseptic conditions in class II biosafety cabinet (Thermo scientific, USA). The floor of the biosafety cabinet was thoroughly sprayed and swabbed with 70 % ethanol. The surface of all the vessels and other instruments used for the study were also cleaned with ethanol. The chamber was then sterilized within built UV rays continuously for 1h before inoculation. Hands and arms inside the inoculation chamber were swabbed with ethanol before inoculation. For the present investigation Dulbecco Modified Eagle Medium (DMEM) supplemented with 10 % heat inactivated fetal bovine serum (FBS), Penicillin-Streptomycin and 0.37 % sodium bicarbonate was used. The powdered DMEM was prepared with sterilized double distilled water as per the manufacturer's recommendation. The prepared media, then subjected to filtering sterilization using 0.2 µ Whatman filter paper [13]. Further, for the present study three different cell lines of varying origin were selected. The A549, HeLa and MCF-7 cells were used for determining the IC_{50} value of newly synthesized series **9a-d** and **10a-d** by MTT, trypan blue LDH leak and colonogenic assays. The cells were treated using increasing concentrations of compounds **9a-d** and **10a-d** (0,

View Article Online
DOI: 10.1039/C7MD00593H

5, 10, 25, 50 and 100 μM in DMSO) at various time intervals (0-48 h) and further used for experiments. Appropriate vehicle control and cisplatin as positive control were used and each experiment was repeated for a minimum of three independent times.

4.3.2. MTT assay.

For the evaluation of the effect of compounds **9a-d** and **10a-d** on cell proliferation of A549, HeLa and MCF-7 cells, the MTT assay was performed as described earlier [13]. Cells, growing in exponential phase were seeded into 96-well plates in triplicates at an initial density of 3×10^4 cells per well in 100 μl of complete medium. Following 16 h incubation, compounds **9a-d** and **10a-d** were added to the culture medium at 0, 5, 10, 25, 50 and 100 μM concentrations with appropriate controls and blanks. Cells were incubated for 48 h. Later, 10 μl MTT (5 mg/ml) reagent was added and incubated for 4 h at 37 ^{o}C. For solubilization of the resultant 5-(4,5-dimethyl thiazol-2-yl)-1,3-diphenyl blue (formazan) product which obtained by reduction of MTT after the incubation period, 100 μl of DMSO was added. The absorbance was measured using a multimode reader at a test wavelength of 570 nm and a reference wavelength of 630 nm. Data obtained are expressed as the percentage of control mean ± standard error of the mean (SEM) of triplicate values.

4.3.3. Trypan blue dye exclusion assay.

The effects of the compounds **9a-d** and **10a-d** on A549, HeLa and MCF-7cells were determined by trypan blue dye exclusion assay [13, 14]. Then the A549, HeLa and MCF-7 cells were cultured and treated with or without compounds were collected after 48 h. The viable cells were counted by resuspending the cells in 0.4 % trypan blue and the IC_{50} values were estimated.

4.3.4. LDH release assay.

View Article Online
DOI: 10.1039/C7MD00593H

The LDH assay was performed to assess the LDH release by treating with compounds **9a-d** and **10a-d** (0, 5, 10, 25, 50 and 100 μM in DMSO) on both A549, HeLa and MCF-7 cells after 48 h of incubation as described earlier [14]. The cells were lysed using 0.1 % "Triton-×100" in PBS. The amount of LDH released in both culture media and cell lysate was measured at 490 nm using an ELISA reader. The percentage of LDH release was calculated as LDH release in the media (LDH release in media + intracellular LDH release) × 100.

4.3.5. Colony formation assay.

The colony formation assay has been the gold standard for determining the anti-neoplastic effects of cytotoxic compounds on cancer cell proliferation *in vitro* and it was performed as described earlier for the potent compound **9d** against A549 cells [22-24]. In brief, the cells were cultured in T-25 tissue culture flasks for 24 h and exposed to test compounds for **9d** at 10 μM and 20 μM concentrations. The cells were then trypsinized, counted and seeded into a six well plate at appropriate densities and cultured for 8 days. Colonies were fixed with methanol, stained with crystal violet (0.4 g/l), photographed, analyzed and counted using ImageJ (v1.48) software.

4.3.6. Migration assay.

A549 cells were cultured in six well plate a until they reached a confluence of 60-70 %. A scratch was made to form a wound using micropipette and the monolayer was washed with growth medium. Then 2 ml medium containing different concentrations of test drugs was added to the respective wells, incubated for 48 h, fixed with chilled 70 % ethanol and stained with crystal violet (0.4 g/l). Images were taken from random fields at regular time intervals using an inverted microscope (Bresser, Biolux). Finally, percentage of cell migration was calculated by comparing the final gap width to initial gap width [13, 25, 26].

View Article Online
DOI: 10.1039/C7MD00593H

4.3.7. *In vivo* rVEGF$_{165}$ induced chorioallontoic membrane (CAM) assay.

The *In vivo* CAM model was performed to evaluate anti-angiogenesis activity with slight modifications as described previously. In brief, fertilized eggs were incubated, windows were made on the 3rd day, and filter paper discs loaded with test compound **9d** (10 μM) was placed on CAMs. Then the eggs were reincubated after proper sealing for 3-4 days. Finally, the eggs were opened and changes in the MVD were photographed using Sony steady shot DSC-W610 camera. Based on the changes in the MVD, the inhibition of angiogenesis was evaluated [19, 21, 27, 28].

4.3.8. *In vivo / ex vivo* rVEGF$_{165}$ induced CAM assay.

To confirm the angioprevention effect of compound **9d**, the *in vitro* / *ex vivo* shell less CAM assay was performed. In brief, the two days old fertilized incubated eggs were cracked out and the contents were poured onto a sterilized condiment cup covered with saran wrap. The egg preparations were covered with a sterilized petri dish and re-incubated at the humidified condition at 37 ^{o}C. On day 4th the egg preparations were impregnated with sterile filter discs containing rVEGF$_{165}$ followed by the treatment with compound. After 72 h of incubation the change in the vascularization in both treated and untreated egg preparations was photographed using Sony steady shot DSC-W610 camera and the blood vessels were quantified [20].

4.3.9. *In vivo* CAM xenograft assay.

The *in vivo* CAM xenograft model to assess angiogenesis was developed with slight modification as described previously [21, 29]. In brief, the cell line used for the present assay is human lung adenocarcinoma (A549), which was cultured as described previously. The fertilized Giriraja breed hen's eggs were procured from local market. The eggs were wiped with 70 % alcohol thoroughly and maintained at the 37 ^{o}C under the humidified condition for the development of the embryo. Under aseptic condition 50 μl of extracellular matrix (ECM) gel was

View Article Online
DOI: 10.1039/C7MD00593H

coated on the bottom of plastic ring of dimension 4mm × 4mm (height × diameter). A small window was made in the fertilized eggs on the 6th day of fertilization and about 1ml of albumin was drawn carefully without damaging the CAM, using sterilized syringe. The plastic rings with ECM gel were placed on the growing CAM under sterilized condition. The rings were then adsorbed with 5×10^6 A549 cell suspension along with $rVEGF_{165}$ (10 ng/ml). The window was sealed using a sterile serine wrap and again kept for incubation. The eggs were opened on the12th day and tumor was separated from CAM, photographed and histological sections were processed for MVD count.

4.3.10. Changes in the morphology of cell line by Giemsa staining.

The untreated and treated cells with the compound **9d** were trypsinized and stained with 20X Giemsa stock solution at a stain to cell suspension ratio of 1:10. Morphology and apoptotic body formations were evaluated by control versus compound **9d** treated cells. Then the cells were viewed under the 40X objective of the microscope (Biolux, Bresser Germany) mounted with MagCam, Magnus Analytics and finally the images were analyzed with ImageJ software [14, 19, 30].

4.3.11. Endonuclease assay.

The endonuclease assay was performed to assess the compounds induced DNase activation by the methods described earlier [20]. Briefly, one portion of cytosolic extracts of A549 cells prepared in lysis buffer (10 mM tris-hydrochloric acid, pH 8.0, 0.1 mM EGTA and 0.1 % β-mercaptoethanol and protease inhibitors) was treated with camptothecin, second potion with compound **9d** and the third potion with untreated. Then 1 % agarose which contains 10 µg/ml ethidium bromide and 50 µg/ml of hot denatured salmon-sperm DNA was plated on glass petri dishes and allowed to solidify at room temperature. Wells were prepared in

View Article Online
DOI: 10.1039/C7MD00593H

petri dishes by suction pressure and equal amounts of protein (500 µg) from camptothecin, compound **9d** and control were added. The above cytosolic extracts were added to the wells and incubated for 12-18 h at 37 ^{o}C in a humidified chamber. The endonuclease assay was performed and the DNA cleavage zone was assessed [20]. Then the DNA cleavage zone was visualized under SYBR green view of Bio-Rad Gel documentation^{TM}XR + Imaging system and photographed.

4.3.12. DNA fragmentation assay.

Lambda phage DNA was treated with different concentration of the compound **9d**, then the DNA was resolved in 0.8 % agarose gel and fragmentation of treated DNA was observed and documented under Syngene Ingenius Gel documentation and Imaging system [13, 31].

4.3.13. Immunoblots.

The whole cell lysates were prepared from compound **9d** treated and untreated A549 cells using RIPA buffer (100 mM tris pH 7.5, 140 mM sodium chloride, 0.1 % SDS, 5 mM EDTA, 1 % "Triton-× 100", 0.5 % sodium deoxycholate, 0.5 mM PMSF and protease inhibitor cocktail). Cell lysates concentration was determined by using Biospectrophotometer and 30 µg of lysates were resolved with 12 % sodium dodecyl sulfate polyacrylamide gel electrophoresis and transferred to polyvinylidene difluoride. Immunoblot analysis was carried out for VEGF-A, caspase-3 (Santacruz Biotechnology, USA) and β-actin (BD Bioscience, USA) [13].

4.3.14. Annexin v apoptosis by flow cytometry.

The A549 cells were seeded into six well plate and incubated at 37 °C for 24 h. The cells were treated with the IC_{50} concentration of the compound **9d** for12-15 h, trypsinized and taken into 15 ml tubes. Then the cells were washed with 1× DPBS, re-suspended in 1X binding buffer solution at a concentration of 1×10^{6} cells/ml. Further, 100 µl of the cell suspension was taken in

View Article Online
DOI: 10.1039/C7MD00593H

a 1.5 ml tube, 5 µl of FITC-Annexin V was added and incubated for 15 minutes at room temperature (25 °C) in the dark. Then 5 µl of PI and 400 µl of the 1X binding buffer were added to each tube and vortexed gently. Finally, the samples were analyzed by BD Accuri C6 Flow Cytometer, BD Biosciences [22, 32-36].

4.3.15. Regulation of cell cycle arrest.

For the cell cycle analysis, cells were seeded into six well plate and incubated at 37 °C for 24 h. Then the cells were treated with the IC_{50} concentration of the compound **9d** for 16 h, trypsinized and taken into 15 ml tubes. Further, the cells were washed with 1× DPBS, fixed in chilled 70 % ethanol (-20 °C), then twice with 1× DPBS, resuspended in 400 µl PI-RNase solution per million cells and taken into 1.5 ml tubes. Finally, the samples were mixed well and analyzed by BD Accuri C6 Flow Cytometer, BD Biosciences [22, 37, 38].

***5. In silico* study.**

The chembiodraw Ultra 14.0 software was used for building the ligands, including all hydrogen atoms. The compounds used for docking was converted into 3D with ChemBio3D Ultra 14.0. For the purpose of *in silico* study, autodock tools program was used. A conformational search of the ligand, which is considered as one of the applications of multi conformer docking, is first approved, and all related low energy conformations are then inflexibly located in the binding site. In order to consider the rigid conformer, the rotational and translational degrees of freedom were allowed. A series of shape based filters are used by the autodock process and Gaussian shape fitting is the building block, in which scoring conformation depends on binding energies. By using autodock tools-1.5.6 the *in silico* study of the inhibitors with VEGFR kinase domain from VEGF (PDB-2xir: A), was performed. In three dimensional atomic coordinates the proteins and ligands were downloaded and prepared for molecular

View Article Online
DOI: 10.1039/C7MD00593H

docking. A method of Lamarckian genetic algorithm (LGA) was applied in the program which is used to identify appropriate binding modes and conformation of the ligands molecules. One of the major process of *in silico* study is the addition of the polar hydrogen atoms and the assigning of kollman charges to the protein using autodock tools. Type grid maps have been assigned to every single atom in the protein and the ligands. Through the study a calculation has been done for the desolation maps and additional electrostatic. Using LGA, molecular docking simulations were performed as the search algorithm. With the help of PyMol program, all molecular modeling experiments are carried out with carton and ribbon models as shown in figure.1 [39-41].

6. Statistical analysis

Statistical analysis data are shown as mean ± SEM, and analysis involved use of SPSS 17.0 by one-way ANOVA followed by student's t-test. Statistically significant values were represented as *$p < 0.05$ and **$p < 0.01$.

7. Conflict of interest statement

The authors declare that there are no conflicts of interest

Acknowledgements

Yasser Hussein Eissa Mohammed is thankful to the University of Hajja, Yemen, for providing financial assistance under the teacher's fellowship. Special thanks to Cytxon Biosolutions pvt. Ltd, Hubballi, India for cell culture assistance for the work. Also, the author expresses his thanks to Scintilla BIO-MARC pvt. Ltd, Bangalore, India for cell culture assistance for the work. Shaukath Ara Khanum expresses. Sincere gratitude to the Government of Karnataka, Vision Group on Science and Technology, Bangalore for the financial assistance

View Article Online
DOI: 10.1039/C7MD00593H

and support [VGST/CISEE/ 2012-13/282 dated 16th March 2013] and UGC, New Delhi under the Major Research Project Scheme [F.39/737/2010 (SR)].

Scheme 1. Synthesis of novel benzophenone analogs (**9a–d** and **10a-d**).

Table 1: IC_{50} values of compounds 6a-m calculated based upon MTT, LDH leak and Trypan at 48 h in A-459, Hela and MCF-7 cells.

Table2: The dock score results of the N'-(2-(2-chloro-6-fluoro-4-(4-methylbenzoyl)phenoxy)acetyl)-1-methyl-1H-imidazole-4-carbohydrazide with VEGFr [PDB code: VEGFr (2xir:A)].

Figure.1. Schematic representation of the docking process.

Figure.2. The basic structure N'-(2-(2-chloro-6-fluoro-4-(4-methylbenzoyl)phenoxy)acetyl)-1-methyl-1H-imidazole-4-carbohydrazide.

Figure.3. Compound **9d** exhibits the prolonged activity**.** a) A549 cells were pretreated with compound **9d** (25 μM and 50μM) for 6 h and incubated for the period of 12 days to form colonies. b) Mask colony counts of untreated, cisplatin 25 μM and compound **9d** 25μM. c) Graphical representation of restraining of colony formation. Statistical significant values were expressed *$p < 0.05$ and **$p < 0.01$.

Figure.4. a) Compound **9d** exhibited an inhibition of migration of A549 cells as 78.83 % and 15.59 % at 50 μM and 25 μM respectively, whereas the standard cisplatin shown inhibition of 76.13 % and 20.25 % at 50 μM and 25 μM respectively. b) Graphical representation of cancer cell Inhibition of A549 cell migration. c) The A549 monolayers were scratched to form wound and treated with compound **9d** for 48 h and pictures of the migrated cells were taken using a microscope with a 10X objective (total magnification 100X. d) Graphical representation of cancer cell migration; statistically significant values are expressed as *$p < 0.05$ and **$p < 0.01$.

View Article Online
DOI: 10.1039/C7MD00593H

Figure.5. *In vivo* CAM photographs represent the inhibition of neovessel formation. a) The *In vivo* CAM photos exhibit the angiopreventive effect of compound **9d** compared to $VEGF_{165}$ and standard cisplatin $VEGF_{165}$ treated CAM. b) The *ex vivo* CAM photos exhibits the angiopreventive effect of compound **9d** compared to $VEGF_{165}$ and standard cisplatin $VEGF_{165}$ treated CAM. c) Micrographs of H and E stained exhibits tumor inhibitory potential in A549 xenograft tumor sections confirming the reduced MVD/HPF with compound **9d**. Magnification of the micrograph is 40×. d) Graphical representation of the MVD count in untreated, standard cisplatin, and compound **9d** treated *in vivo* CAM. e) Graphical representation of the MVD count in untreated, standard cisplatin, and compound **9d** treated *ex vivo* CAM. F) Percentage of A549 tumor MVD inhibition. Statistically significant values are expressed as *$p < 0.05$ and **$p < 0.01$.

Figure.6. Giemsa stained A549 cells showing the morphological changes, such as irregular shape, membrane blabbing and formation of apoptotic bodies in standard cisplatin and compound **9d** treated cells compared to untreated cells.

Figure.7. a) Endonuclease assay showing DNA lysis zone in cytosolic fractions treated with camptothecin and compound **9d** as observed compared to the control. b) The graphical representation of the percentage of the DNA lysis zone in cytosolic fractions. c) Reduction in translational VEGF expression compared to control. d) Agarose gel electrophoresis for DNA fragmentation assay (apoptotic ladder) showing lane 1 as control, lane 2 as marker (DNA ladder) and cells treated with compound **9d** in lane 3. Statistically significant values are expressed as *$p < 0.05$ and **$p < 0.01$.

View Article Online
DOI: 10.1039/C7MD00593H

Figure.8. Compound **9d** promotes the apoptotic cell death. FACS analysis showing the increased number of apoptotic cells in the compound **9d** treated A549 cells. a) The test sample treated cells contained 0.68 % cells in early apoptosis and 48.4 % cells in the late apoptosis stage. b) Graphical representation percentage of cells undergoing apoptosis. c) Compound **9d** promote the apoptotic cell death by caspase-3 activation. A molecular event of compound **9d** exhibited tumor regression was analyzed by immunoblot. Statistically significant values are expressed as *p < 0.05 and **p < 0.01.

Figure.9. a) Cell cycle arrest in G2 phase was observed upon treatment with compound **9d** (85 μM) as an increase in the percentage of cells in G0/G1 Gate was observed. b) The graphical representation of the percentage of cells in G0/G1, G2/M and S-phase of the cell cycle. Statistically significant values are expressed as *p < 0.05 and **p < 0.01.

Figure. 10. Compound **9d** showed minimum binding energy with rVEGF at the confirmation **S2** with the lowest binding energy of -7.66 kJ mol^{-1}; Statistically significant values are expressed as *p < 0.05 and **p < 0.01.

Figure .11. Compound **9d** interacts with VEGFr for cancer regression *in silico*. a) Enfolding of molecules **9d** in the active site pocket of VEGFr complexes. b) Ribbon models of $VEGF_r$ catalytic domain and ligand molecules compound **9d** complexes. c) Hydrogen bond interaction of the ligand molecule compound **9d** with VEGFr. d) The 3D interactions analysis of compound **9d** with VEGFr.

Figure .12. Schematic representation of compound **9d** exhibited angiogenesis inhibition and induced apoptosis.

References

View Article Online
DOI: 10.1039/C7MD00593H

[1] V. Vigneshwaran, P. Thirusangu, S. Madhusudana, V. Krishna, S.N. Pramod, B.T. Prabhakar, The latex sap of the 'Old World Plant'Lagenariasiceraria with potent lectin activity mitigates neoplastic malignancy targeting neovasculature and cell death, IntImmunopharmacol, 39 (2016) 158-171.

[2] B.V. Avin, T. Prabhu, C.K. Ramesh, V. Vigneshwaran, M. Riaz, K. Jayashree, B.T. Prabhakar, New role of lupeol in reticence of angiogenesis, the cellular parameter of neoplastic progression in tumorigenesis models through altered gene expression, Biochemical and Biophysical Research Communications. 448 (2014) 139-144.

[3] P. Thirusangu, V. Vigneshwaran, B.V.Avin, H. Rakesh, H.M. Vikas, B.T. Prabhakar, Scutellarein antagonizes the tumorigenesis by modulating cytokine VEGF mediated neoangiogenesis and DFF-40 actuated nucleosomal degradation, Biochemical and Biophysical Research Communications. 484 (2017) 85-92.

[4] B.Stoelcker, B.Ruhland, T.Hehlgans, H.Bluethmann, T. Luther, D.N.Männel, Tumor necrosis factor induces tumor necrosis via tumor necrosis factor receptor type 1-expressing endothelial cells of the tumor vasculature, The American Journal of Pthology. 4 (2000)1171-1176.

[5] D.R.Senger, C.A.Perruzzi, J.Feder, H.F. Dvorak, A highly conserved vascular permeability factor secreted by a variety of human and rodent tumor cell lines, Cancer research. 11 (1986) 5629-5632.

[6] H.P. Gerber, T.H. Vu, A.M. Ryan, J. Kowalski, Z.Werb, N. Ferrara, VEGF couples hypertrophic cartilage remodeling, ossification and angiogenesis during endochondral bone formation, Nature Medicine. 6 (1999) 623-628.

[7] P.B. Vermeulen, G. Gasparini, S.B. Fox, M. Toi, L. Martin, P. McCulloch, F. Pezzella, G. Viale, N. Weidner, A.L. Harris, L. Y. Dirix, Quantification of angiogenesis in solid human

View Article Online
DOI: 10.1039/C7MD00593H

tumours: an international consensus on the methodology and criteria of evaluation, European Journal of Cancer. 14 (1996) 2474-2484.

[8] G. Bergers, D. Hanahan, L.M. Coussens, Angiogenesis and apoptosis are cellular parameters of neoplastic progression in transgenic mouse models of tumorigenesis, International Journal of Developmental Biology. 42 (1998) 995-1002.

[9] D. Sloane, Cancer epidemiology in the United States: racial, social, and economic factors, Cancer Epidemiology. 471 (2009) 65-83.

[10] K. Hotta, H. Ueoka, New cytotoxic agents: a review of the literature, Critical Reviews in Oncology/Hematology. 55 (2005) 45-65.

[11] T. Prashanth, P. Thirusangu, B.V. Avin, V.L. Ranganatha, B.T. Prabhakar, S.A. Khanum, Synthesis and evaluation of novel benzophenone-thiazole derivatives as potent VEGF-A inhibitors, European Journal of Medicinal Chemistry. 87 (2014) 274-283.

[12] M. Al-Ghorbani, P. Thirusangu, H.D. Gurupadaswamy, V. Girish, H.S. Neralagundi, B.T. Prabhakar, S.A. Khanum, Synthesis and antiproliferative activity of benzophenone tagged pyridine analogues towards activation of caspase activated DNase mediated nuclear fragmentation in Dalton's lymphoma, Bioorganic Chemistry. 65 (2016) 73-81.

[13] Y.H. Eissa Mohammed, P. Thirusangu, S.A. Khanum, The anti-invasive role of novel synthesized pyridazine hydrazide appended phenoxy acetic acid against neoplastic development targeting matrix metallo proteases, Biomedicine and Pharmacotherapy. 95 (2017) 375.

[14] B.R. Vijay Avin, P. Thirusangu, V.L. Ranganatha, A. Firdouse, B.T. Prabhakar, S.A. Khanum, Synthesis and tumor inhibitory activity of novel coumarin analogs targeting angiogenesis and apoptosis, European Journal of Medicinal Chemistry. 75 (2014) 211-221.

View Article Online
DOI: 10.1039/C7MD00593H

[15] V.L. Ranganath, B.R.V. Avin, P. Thirusangu, T. Prashanth, B.T. Prabhakar, S.A. Khanum, Synthesis, angiopreventive activity, and in vivo tumor inhibition of novel benzophenoneebenzimidazole analogs, Life Sciences. 93 (2013) 904-911.

[16] E. Kumazawa, K. Hirotani, S. Clifford Burford, K. Kawaagoe, T. Miwa, I. Mitsui, A. Ejima, Synthesis and antitumor activity of novel benzophenone derivatives, Chemical and Pharmaceutical Bulletin. 45 (1997) 1470-1474.

[17] H.D. Gurupadaswamy, V. Girish, C.V. Kavitha, S.C. Raghavan, S.A. Khanum, Synthesis and evaluation of 2,5-di(4-aryloylaryloxymethyl)- 1,3,4-oxadiazoles as anti-cancer agents, European Journal of Medicinal Chemistry. 63 (2013) 536-543.

[18] B.T. Prabhakar, S.A. Khanum, K. Jayashree, B.P. Salimath, S. Shashikanth, Antitumor and proapoptotic effect of novel synthetic benzophenone analogs in Ehrlich ascites tumor cells, Bioorganic and Medicinal Chemistry Letters. 14 (2006) 435-446.

[19] Y.H.E. Mohammed, V.H. Malojirao, P. Thirusangu, M. Al-Ghorbani, B.T. Prabhakar, S.A. Khanum, The Novel 4-Phenyl-2-Phenoxyacetamide Thiazoles modulates the tumor hypoxia leading to the crackdown of neoangiogenesis and evoking the cell death, European Journal of Medicinal Chemistry. 143 (2018) 1826-1839.

[20] H.D. Gurupadaswamy, T. Prabhu, B.R. Vijay Avin, V. Vigneshwaran, M.V. Prashanth Kumar, T.S. Abhishek, V.L. Ranganatha, S.A. Khanum, B.T. Prabhakar, DAO-9 (2,5-di(4-aryloylaryloxymethyl)-1,3,4-oxadiazole) exhibits p53 induced apoptogenesis through caspase-3 mediated endonuclease activity in murine carcinoma, Biomedicine and Pharmacotherapy. (2014). http://dx.doi.org/10.1016/j.biopha.2014.07.004.

[21] P. Thirusangu, V. Vigneshwaran, T. Prashanth, B.V. Avin, V.H. Malojirao, H. Rakesh, S.A. Khanum, R. Mahmood, B.T. Prabhakar, BP-1T, an antiangiogenic benzophenone-thiazole

View Article Online
DOI: 10.1039/C7MD00593H

pharmacophore, counteracts HIF-1 signalling through p53/MDM2-mediated HIF-1α proteasomal degradation, Angiogenesis. 1 (2017) 55-71.

[22] M. Al-Ghorbani, P. Thirusangu, H.D. Gurupadaswamy, V. Vigneshwaran, Y.H.E. Mohammed, B.T. Prabhakar, S.A. Khanum. Synthesis of novel morpholine conjugated benzophenone analogues and evaluation of antagonistic role against neoplastic development, Bioorganic Chemistry. 71 (2017) 55-66.

[23] N.A. Franken, H.M. Rodermond, J. Stap, J. Haveman, C. Van Bree, Clonogenic assay of cells in vitro, Nature Protocols. 1(2006) 2315.

[24] A. Munshi, M. Hobbs, R.E. Meyn, Clonogenic cell survival assay, Chemosensitivity. 1 (2005) 21-8.

[25] J.H. Chiang, J.S. Yang, C.C. Lu, M.J. Hour, S.J. Chang, T.H. Lee, J.G. Chung. Newly synthesized quinazolinone HMJ-38 suppresses angiogenetic responses and triggers human umbilical vein endothelial cell apoptosis through p53-modulated Fas/death receptor signaling, Toxicology and Applied Pharmacology. 269 (2013) 150-162.

[26] M.G. Lampugnani. Cell migration into a wounded area in vitro, Adhesion Protein Protocols. (1999) pp 177-182.

[27] R. Auerbach, R. Lewis, B. Shinners, L. Kubai, N. Akhtar, Angiogenesis assays: a critical overview, Clinical Chemistry. 1 (2003) 32-40.

[28] K. Norrby, *In vivo* models of angiogenesis, Journal of cellular and molecular medicine, 3 (2006) 588-612.

[29] W. Schneiderhan, F. Diaz, M, Fundel, S. Zhou, M. Siech, C. Hasel, P. Möller, J.E. Gschwend, T. Seufferlein, T. Gress, G. Adler, Pancreatic stellate cells are an important

View Article Online
DOI: 10.1039/C7MD00593H

source of MMP-2 in human pancreatic cancer and accelerate tumor progression in a murine xenograft model and CAM assay, Journal of Cell Science. 3 (2007) 512-519.

[30] P. Perry, S. Wolff, New Giemsa method for the differential staining of sister chromatids, Nature. 5471 (1974) 156-158.

[31] X. Liu, H. Zou, C. Slaughter, X. Wang, DFF, a heterodimeric protein that functions downstream of caspase-3 to trigger DNA fragmentation during apoptosis, Cell. 2 (1997) 175-84.

[32] C. Bai, T. Chen, Y. Cui, T. Gong, X. Peng, H.M. Cui, Effect of high fluorine on the cell cycle and apoptosis of renal cells in chickens, Biological Trace Element Research.1-3 (2010) 173-80.

[33] Y. Fan, J. Cheng, S.A. Vasudevan, R.H. Patel, L. Liang, X. Xu, Y. Zhao, W. Jia, F. Lu, H. Zhang, J.G. Nuchtern, TAK1 inhibitor 5Z-7-oxozeaenol sensitizes neuroblastoma to chemotherapy, Apoptosis. 10 (2013) 1224-1234.

[34] G. Koopman, C.P. Reutelingsperger, G.A. Kuijten, R.M. Keehnen, S.T. Pals, M.H. Van Oers, Annexin V for flow cytometric detection of phosphatidylserine expression on B cells undergoing apoptosis, Blood. 5 (1994) 1415-1420.

[35] I. Vermes, C. Haanen, H. Steffens-Nakken, C. Reutellingsperger, A novel assay for apoptosis flow cytometric detection of phosphatidylserine expression on early apoptotic cells using fluorescein labelled annexin V, Journal of Immunological Methods. 1 (1995) 39-51.

[36] E. Chu, D.M. Koeller, J.L. Casey, J.C. Drake, B.A. Chabner, P.C. Elwood, S. Zinn, C.J. Allegra, Autoregulation of human thymidylate synthase messenger RNA translation by thymidylate synthase, Proceedings of the National Academy of Sciences. 20 (1991) 8977-8981.

View Article Online
DOI: 10.1039/C7MD00593H

[37] P. Pozarowski, Z. Darzynkiewicz, Analysis of cell cycle by flow cytometry, Checkpoint Controls and Cancer. 2 (2004) 301-311.

[38] M.G. Ormerod, B. Tribukait, W. Giaretti, Consensus report of the task force on standardisation of DNA flow cytometry in clinical pathology, Analytical Cellular Pathology. 2 (1998) 103-110.

[39] X.H. Liu, H.F. Liu, J. Chen, Y. Yang, B.A. Song, L.S. Bai, J.X. Liu, H.L. Zhu, X.B. Qi. Synthesis and molecular docking study of novel coumarin derivatives containing 4, 5-dihydropyrazole moiety as potential antitumor agents, Bioorganic and Medicinal Chemistry Letters. 19 (2010) 5705-8.

[40] K.M. Khan, F. Rahim, A. Wadood, N. Kosar, M. Taha, S. Lalani, A. Khan, M.I. Fakhri, M. Junaid, W. Rehman, M. Khan, Synthesis and molecular docking studies of potent α-glucosidase inhibitors based on biscoumarin skeleton, European Journal of Medicinal Chemistry. 81 (2014) 245-252.

[41] A.S. El-Azab, M.A. Al-Omar, A.M. Alaa, N.I. Abdel-Aziz, A.A. Magda, A.M. Aleisa, M.M. Sayed-Ahmed, S.G. Abdel-Hamide, Design, synthesis and biological evaluation of novel quinazoline derivatives as potential antitumor agents: molecular docking study, European Journal of Medicinal Chemistry. 9 (2010) 4188-4198.

View Article Online
DOI: 10.1039/C7MD00593H

The critical role of novel benzophenone analogs on tumor growth inhibitory targeting angiogenesis and apoptosis

Yasser Hussein Eissa Mohammed[1,2] and Shukath Ara Khanum[1].

Figures

Scheme 1

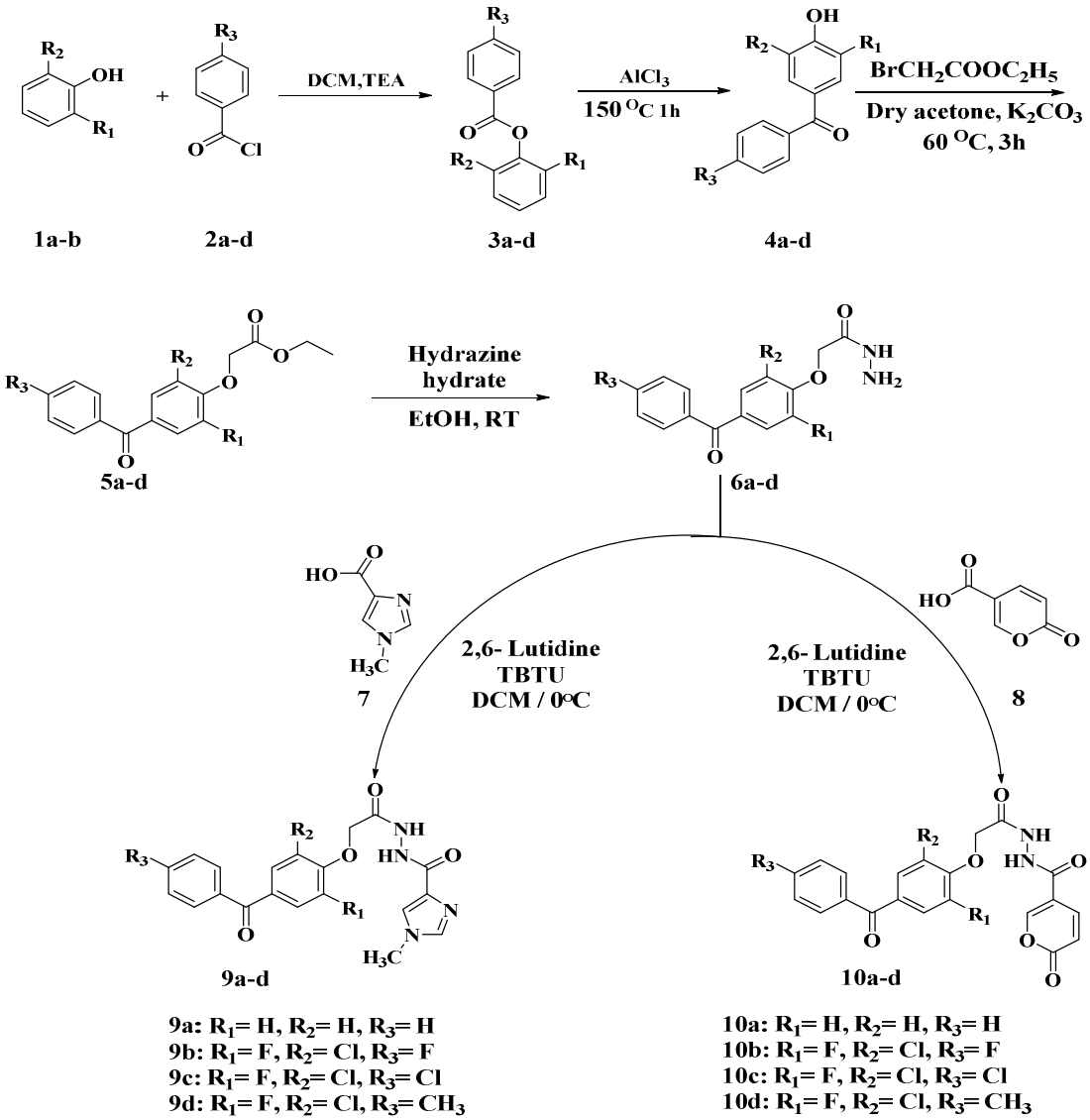

View Article Online
DOI: 10.1039/C7MD00593H

Scheme 1. Synthesis of novel benzophenone analogs (**9a–d** and **10a-d**).

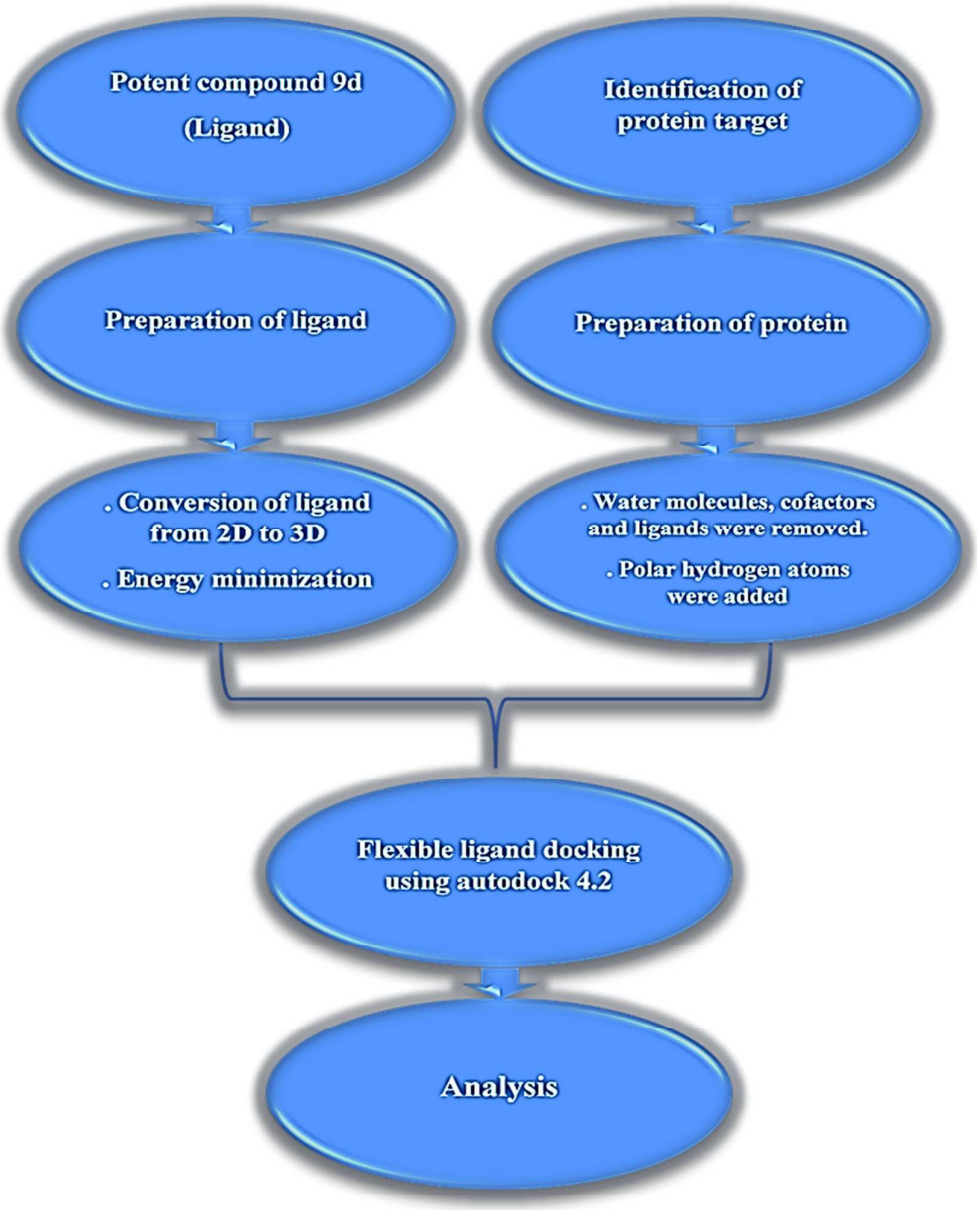

Figure 1. Schematic representation of the docking process.

View Article Online
DOI: 10.1039/C7MD00593H

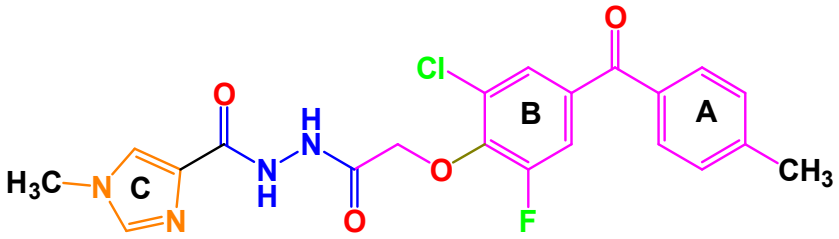

Figure 2. The basic structure of [2-4(4-methyl)benzoyl-2-chloro-6 fluorophenoxy] aceto-N(N-methyl imidazole)carbonyl hydrazide

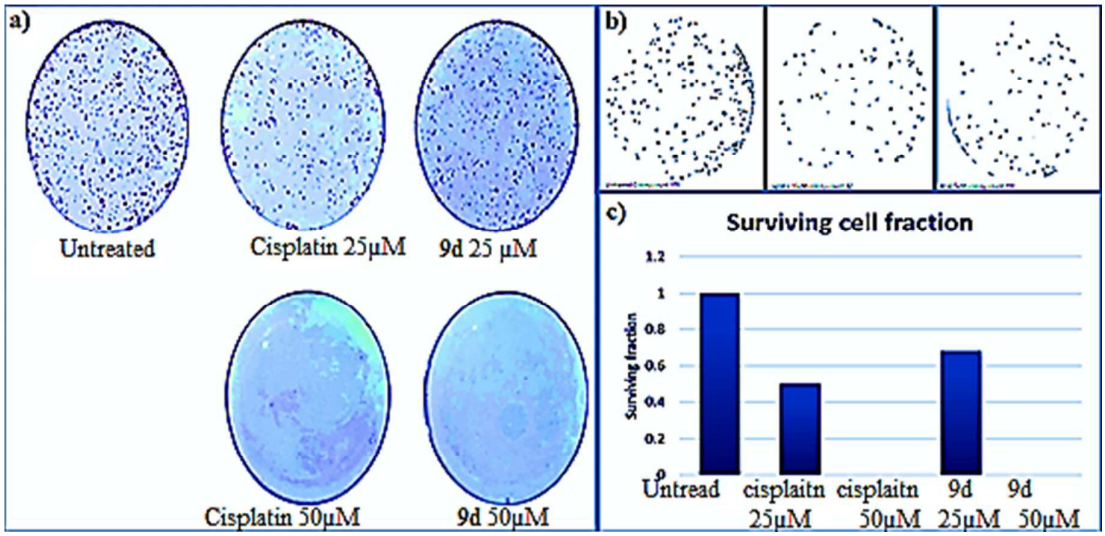

Figure 3. Compound **9d** exhibits the prolonged activity. a) A549 cells were pretreated with **9d** (25 μM and 50 μM) for 6 h and incubated for the period of 12 days to form colonies. b) Mask colony counts of untreated, cisplatin 25 μM and compound **9d** 25 μM. c) Graphical representation of restraining of colony formation. Statistical significant values were expressed *$p < 0.05$ and **$p < 0.01$.

View Article Online
DOI: 10.1039/C7MD00593H

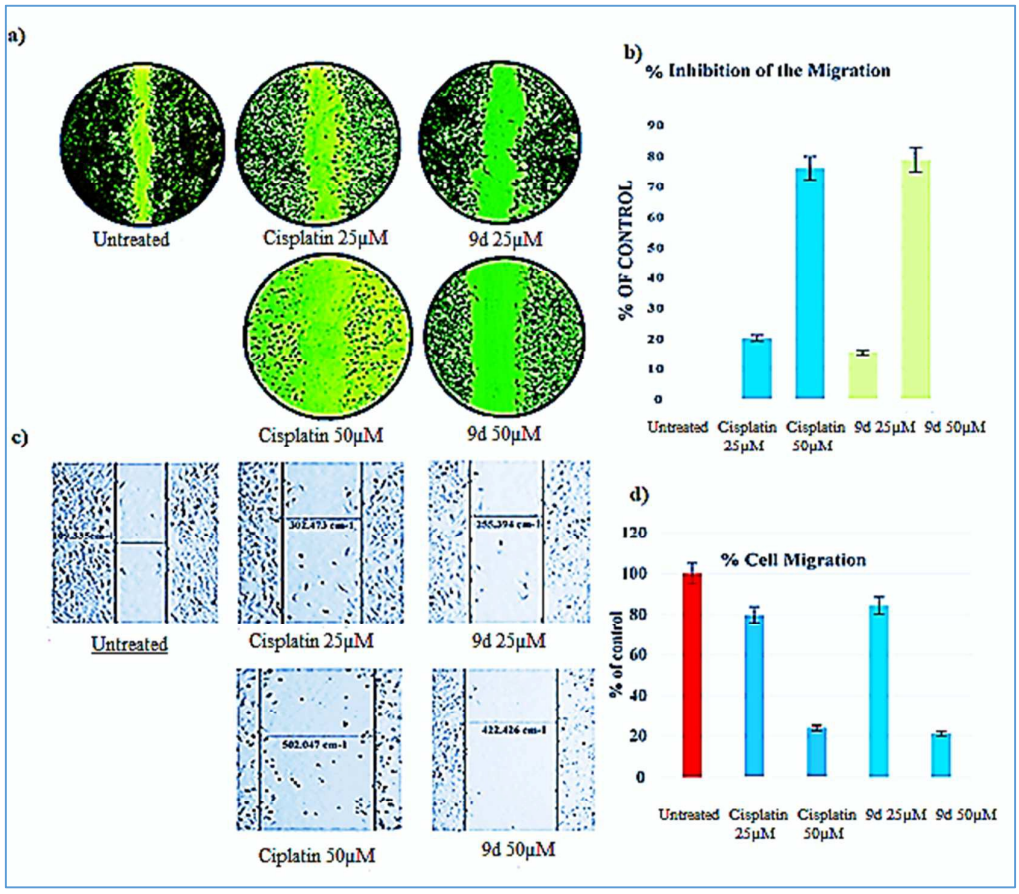

Figure 4. Compound **9d** impairs the cancer cell migration. a) Compound **9d** exhibited an inhibition of migration of A549 cells as 78.83 % and 15.59 % at 50 μM and 25 μM respectively, whereas the standard cisplatin shown inhibition of 76.13 % and 20.25 % at 50 μM and 25μM respectively. b) Graphical representation of cancer cell Inhibition of A549 cell migration. c) The A549 monolayers were scratched to form wound and treated with compound **9d** for 48 h and pictures of the migrated cells were taken using a microscope with a 10X objective (total magnification 100x. d) Graphical representation of cancer cell migration; statistically significant values are expressed as *$p < 0.05$ and **$p < 0.01$.

View Article Online
DOI: 10.1039/C7MD00593H

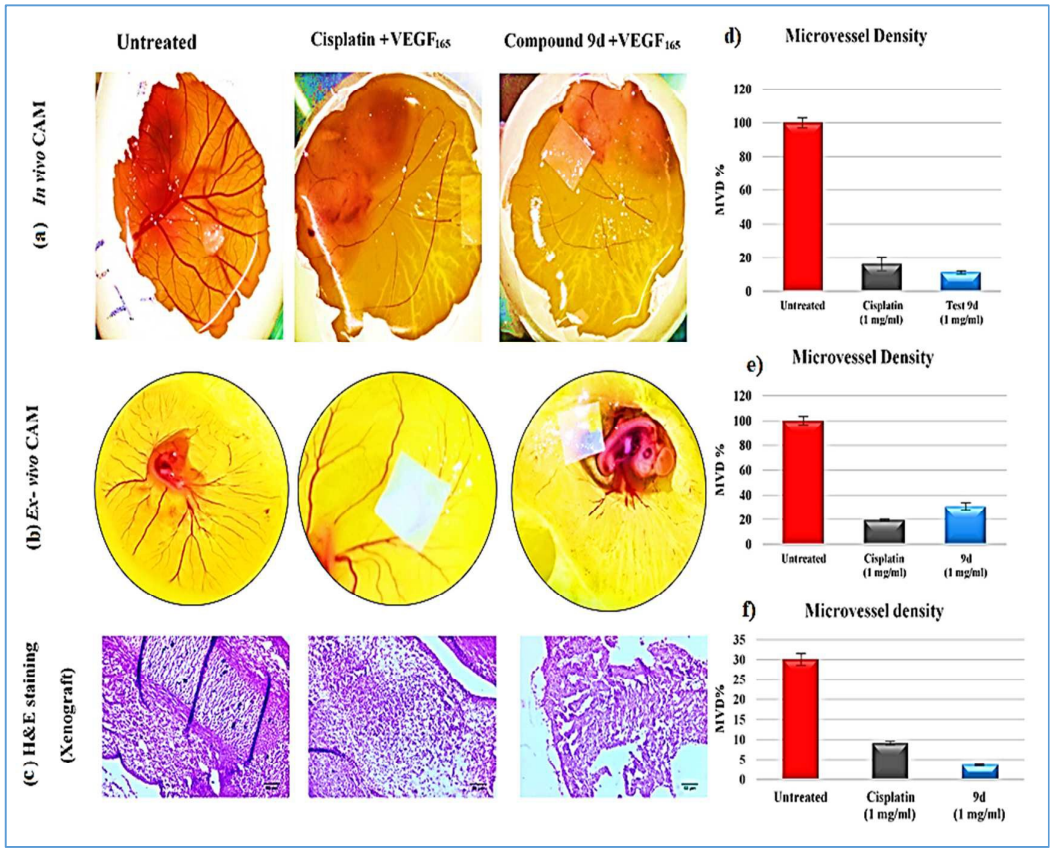

Figure 5. *In vivo* CAM photographs represent the inhibition of neovessel formation. a) The *In vivo* CAM photos exhibit the angiopreventive effect of compound **9d** compared to $VEGF_{165}$ and standard cisplatin $VEGF_{165}$ treated CAM. b) The *ex vivo* CAM photos exhibits the angiopreventive effect of compound **9d** compared to $VEGF_{165}$ and standard cisplatin $VEGF_{165}$ treated CAM. c) Micrographs of H and E stained exhibits tumor inhibitory potential in A549 xenograft tumor sections confirming the reduced MVD/HPF with compound **9d**. Magnification of the micrograph is 40×. d) Graphical representation of the MVD count in untreated, standard cisplatin, and compound **9d** treated *in vivo* CAM. e) Graphical representation of the MVD count in untreated, standard cisplatin, and compound **9d** treated *ex vivo* CAM. f) Percentage of A549 tumor MVD inhibition. Statistically significant values are expressed as *$p < 0.05$ and **$p < 0.01$.

View Article Online
DOI: 10.1039/C7MD00593H

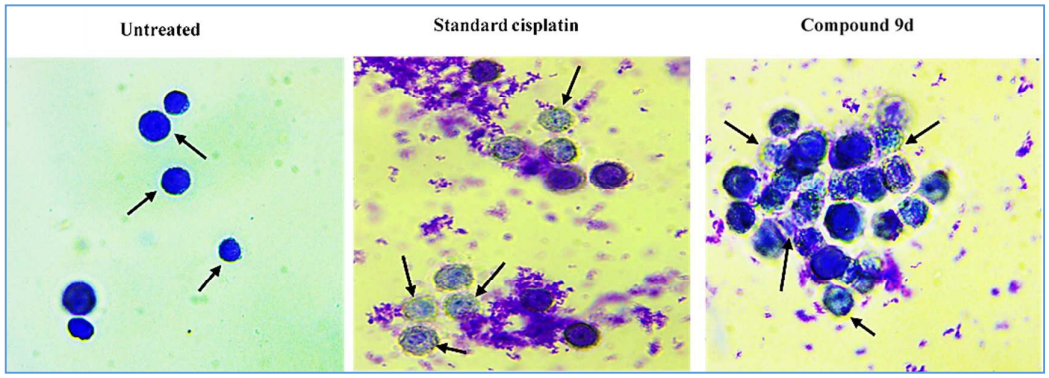

Figure 6. Giemsa stained A549 cells showing the morphological changes, such as irregular shape, membrane blabbing and formation of apoptotic bodies in standard cisplatin and **9d** treated cells compared to untreated cells.

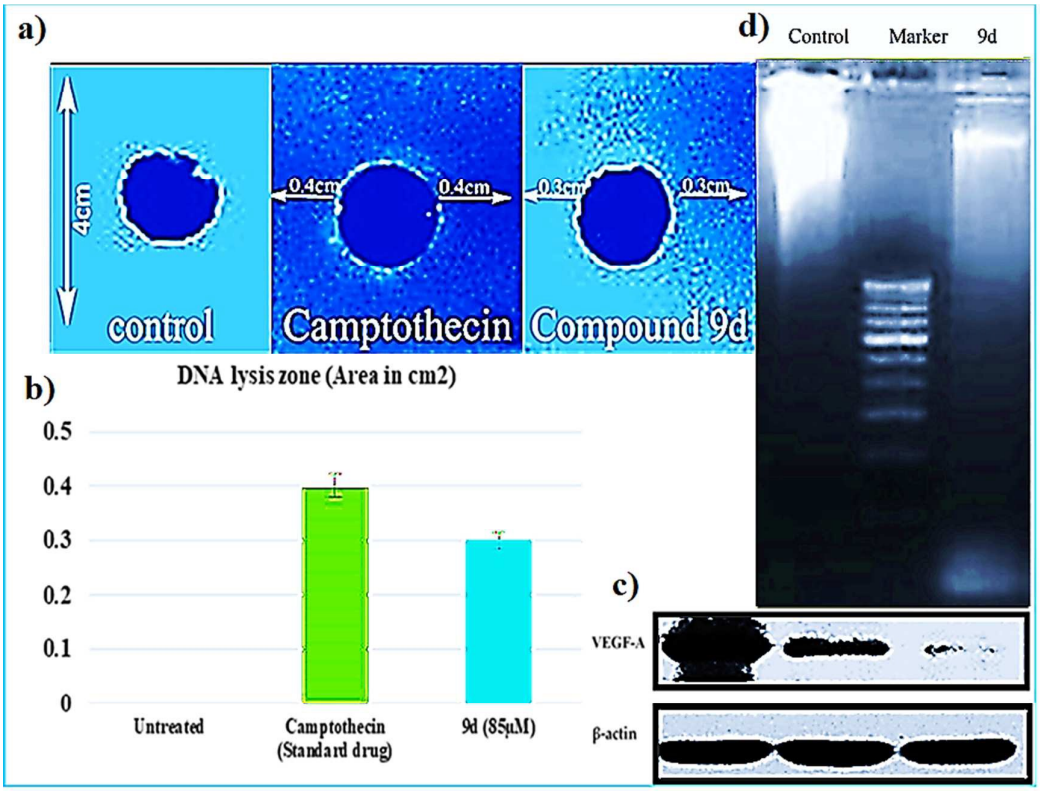

Figure 7. a) Endonuclease assay showing DNA lysis zone in cytosolic fractions treated with camptothecin and compound **9d** as observed compared to the

View Article Online
DOI: 10.1039/C7MD00593H

control. b) The graphical representation of the percentage of the DNA lysis zone in cytosolic fractions. c) Reduction in translational VEGF expression compared to control. d) Agarose gel electrophoresis for DNA fragmentation assay (apoptotic ladder) showing lane 1 as control, lane 2 as marker (DNA ladder) and cells treated with compound **9d** in lane 3. Statistically significant values are expressed as *p < 0.05 and **p < 0.01.

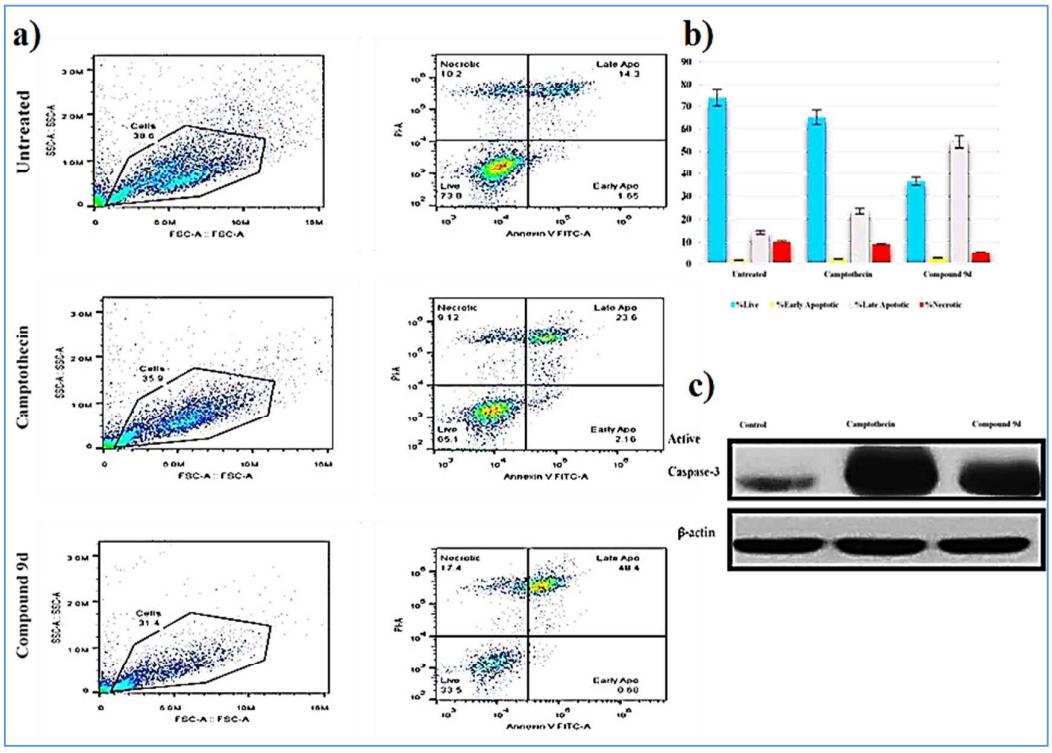

Figure 8. Compound **9d** promotes the apoptotic cell death. FACS analysis showing the increased number of apoptotic cells in the compound **9d** treated A549 cells. a) The compound **9d** treated cells contained 0.68 % cells in early apoptosis and 48.4 % cells in the late apoptosis stage. b) Graphical representation percentage of cells undergoing apoptosis. c) Compound **9d** promote the apoptotic cell death by caspase-3 activation. A molecular event of compound **9d** exhibited tumor regression was analyzed by immunoblot. Statistically significant values are expressed as *p < 0.05 and **p < 0.01.

View Article Online
DOI: 10.1039/C7MD00593H

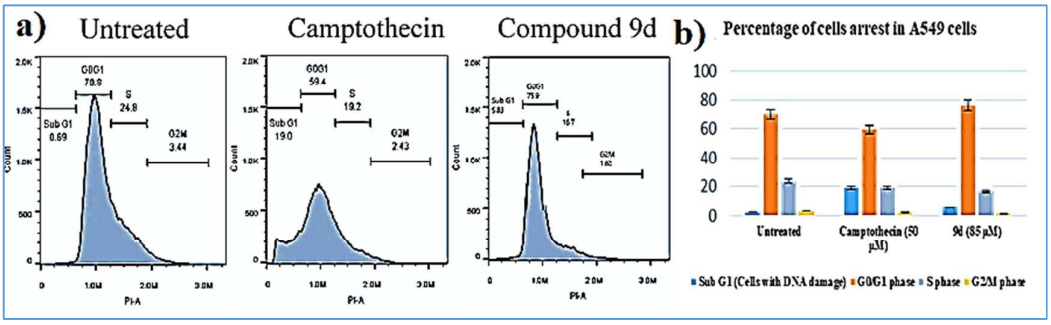

Figure 9. a) Cell cycle arrest in G2 phase was observed upon treatment with compound **9d** (85 µM) as an increase in the percentage of cells in G0/G1 gate was observed. b) The graphical representation of the percentage of cells in G0/G1, G2/M and S-phase of the cell cycle. Statistically significant values are expressed as *p < 0.05 and **p < 0.01.

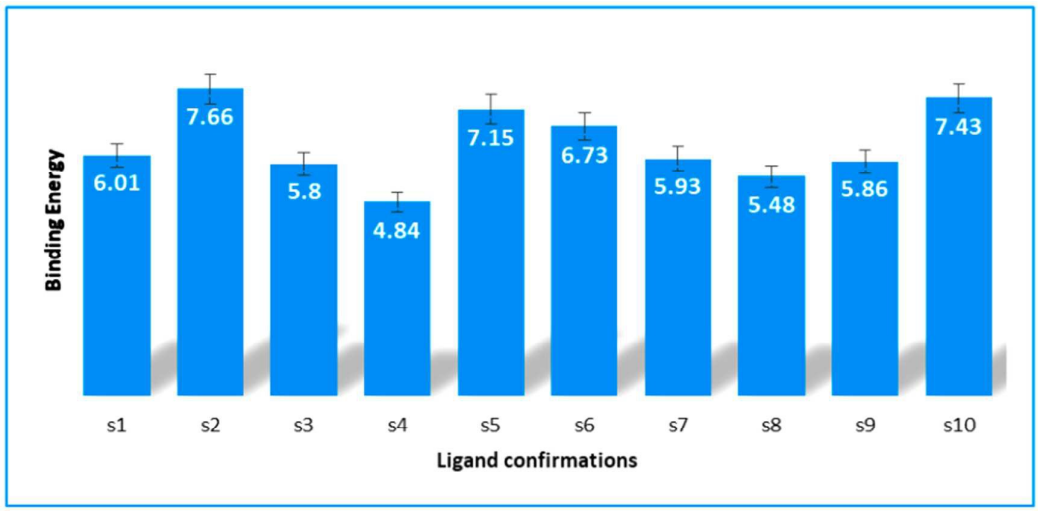

Figure 10. Compound **9d** showed minimum binding energy with rVEGF at the confirmation **S2** with the lowest binding energy of -7.66 kJ/mol; Statistically significant values are expressed as *p < 0.05 and **p < 0.01.

View Article Online
DOI: 10.1039/C7MD00593H

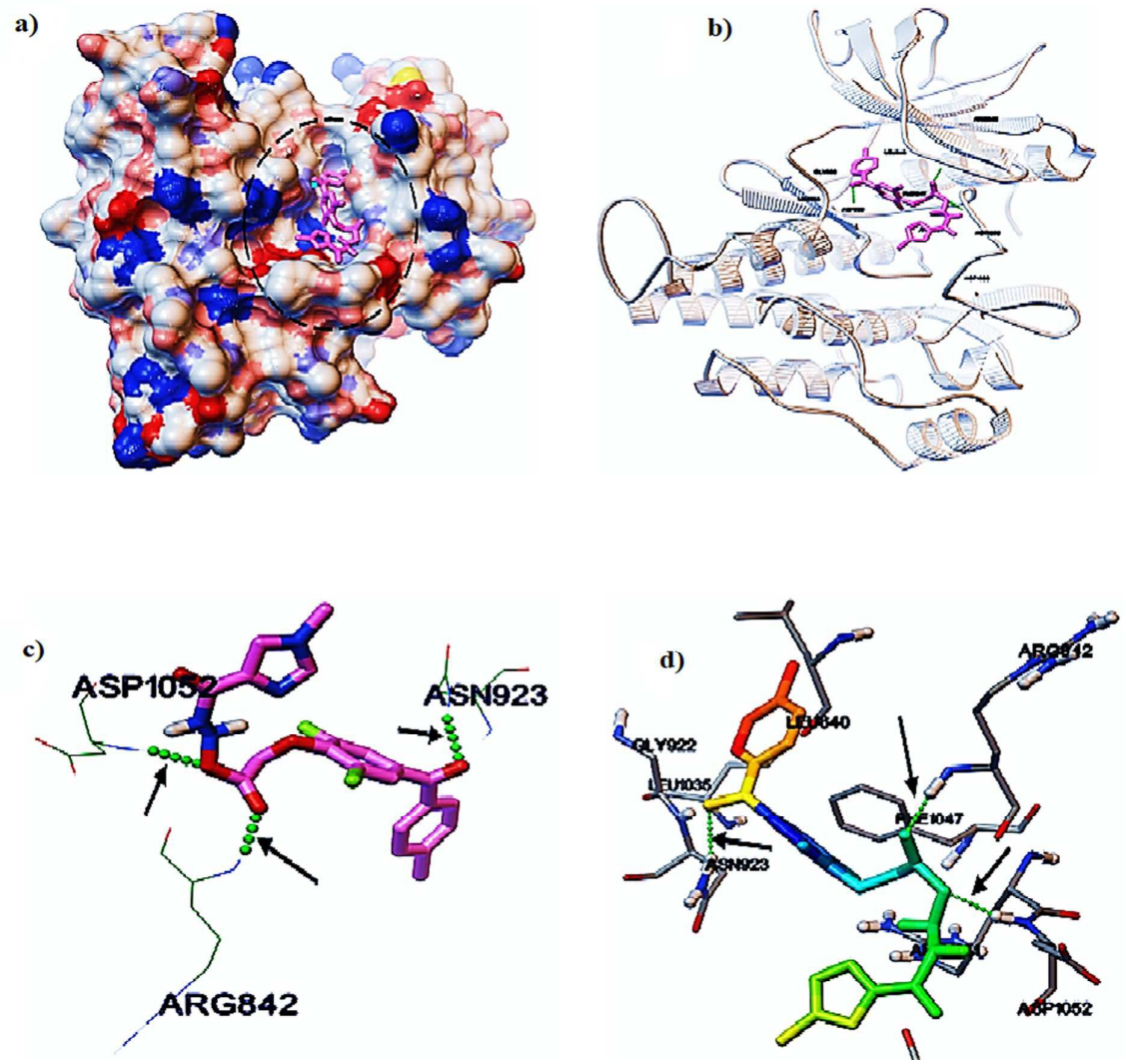

Figure 11. Compound **9d** interacts with VEGFr for cancer regression *in silicon*. a) Enfolding of molecules **9d** in the active site pocket of VEGFr complex. b) Ribbon models of $VEGF_r$ catalytic domain and ligand molecules **9d** complex. c) Hydrogen bond interaction of the ligand molecule **9d** with VEGFr. d) The 3D interactions analysis of **9d** with VEGFr.

View Article Online
DOI: 10.1039/C7MD00593H

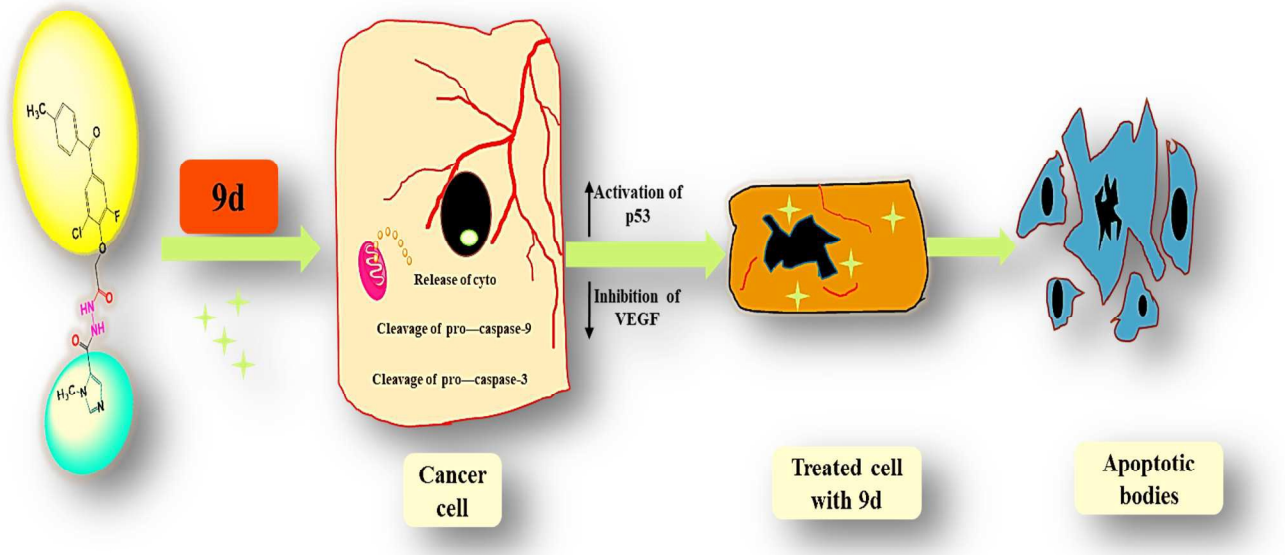

Figure .12. Schematic representation of **9d** exhibited angiogenesis inhibition and induced apoptosis.

Table 1: IC50 values of compounds 6a-m calculated based upon MTT, LDH leak and Trypan at 48 h in A-459, Hela, MCF-7 and NIH-3T3 cells.

	IC50 value (μM) against A-459 cells			IC50 value (μM) against Hela cells			IC50 value (μM) against MCF-7 cells			IC50 value (μM) against NIH-3T3 cells		
	Trypan blue assay IC50 value (μM)	MTT assay IC50 values (μM)	LDH release assay IC50 values (μM)	Trypan blue assay IC50 value (μM)	MTT assay IC50 values (μM)	LDH release assay IC50 values (μM)	Trypan blue assay IC50 value (μM)	MTT assay IC50 values (μM)	LDH release assay IC50 values (μM)	Trypan blue assay IC50 value (μM)	MTT assay IC50 values (μM)	LDH release assay IC50 values (μM)
9a	29.6±1.7	30.6±1.0	31.6±09	33.2±0.3	32.9±1.4	31.9±2.1	29.6±1.7	30.6±1.0	31.6±0.9	98.8±1.1	96.9±1.8	97.4±1.1
9b	39.6±2.1	40.1±0.3	40.7±03	39.9±1.7	42.2±0.4	40.9±1.1	44.6±0.5	45.1±0.7	44.6±1.2	94.2±1.0	89.2±1.3	94.4±1.2
9c	47.3±0.6	49.1±0.9	45.8±1.4	51.6±1.7	536.±0.3	54.5±2.5	47.3±0.6	43.1±0.9	44.4±1.7	90.9±1.3	87.8±1.9	89.3±1.8
9d	**9.6±1.7**	**8.8±0.12**	**9.1±0.5**	**10.2±0.3**	**9.9±1.5**	**10.4±2.1**	**9.5±0.7**	**9.8±1.0**	**9.4±0.9**	**93.8±1.5**	**94.2±1.7**	**94.9±1.7**
10a	96.7 ± 1.6	98.8 ± 2.0	90.9 ± 1.0	89.2 ± 2.0	99.1 ± 1.0	96.1 ± 1.0	92.9 ± 1.6	93.2 ± 2.0	61.1 ± 1.0	84.3±1.3	87.3±1.1	88.2±1.3
10b	56.7 ± 1.1	58.8 ± 2.0	60.2 ± 1.0	59.2 ± 2.0	59.9 ± 1.0	60.1 ± 1.0	62.2 ± 1.2	63.2 ± 1.4	61.1 ± 1.0	85.4±1.4	87.8±1.7	89.8±1.9
10c	86.7 ± 0.6	88.8 ± 2.1	84.9 ± 2.1	89.6 ± 1.2	87.1 ± 1.0	85.1 ± 1.0	90.6 ± 2.1	86.2 ± 0.5	83.8 ± 1.4	79.3±1.5	77.6±1.7	78.6±1.6
10d	19.6±1.7	22.6±1.2	21.4±0.9	26.2±0.3	20.9±2.4	26.9±0.1	29.1±1.0	23.6±2.0	24.2±1.9	30.8±1.1	28.9±0.8	32.1±2.1
Cisplatin	7.7±0.5	7.9±0.5	7.4±0.5	8.6±0.7	8.9±1.0	8.8±2.1	6.4±1.5	6.5±1.5	6.8±0.1	94.4±1.7	93.2±1.6	91.1±1.7

Cisplatin is used a positive control and DMSO is used as a vehicle control which showed very negligible cytotoxicity. Values are indicated in mean ± SE (SEM).

Table.2: The dock score results of the N'-(2-(2-chloro-6-fluoro-4-(4-methylbenzoyl)phenoxy)acetyl)-1-methyl-1H-imidazole-4-carbohydrazide with vascular endothelial growth factor PDB Code: VEGFr (2xir:A).

Conformation	Binding energy (kJ mol^{-1})	Ligand efficiency	Inhibition constant	vdW+H-bond+desolv energy	No. of H- bonds	Bonding residues	Bond length (Å)
S1	-6.01	-0.19	39.35	-8.77	-	-	1.991
S2	**-7.66**	**-0.24**	**2.43**	**-10.14**	**2**	**2xir:A : ARG842:HN: Lig: LIG1: O:** **2xir:A: ASN923:HD21: Lig: LIG1: O:** **2xir:A: ASP1052:HN: Lig: LIG1: O:**	**1.739** **1.987** **1.931**
S3	-5.8	-0.18	35.76	-8.47	1	2xir:A : ASP875:O: Lig: LIG1: H:	2.197
S4	-4.84	-0.15	285.4	-7.52	-	-	-
S5	-7.15	-0.22	5.76	-9.71	2	2xir:A :LYS1023:O: Lig: LIG1: H: 2xir:A:ARG1027:HH22: Lig: LIG1: O:	2.082 2.033
S6	-6.73	-0.21	11.66	-9.25	3	2xir:A : ASN923:HN: Lig: LIG1: O: 2xir:A: ASN923:HD21: Lig: LIG1: O: 2xir:A: ASP1052:HN: Lig: LIG1: O:	1.773 1.914 1.869
S7	-5.93	-0.19	45.13	-8.61	1	2xir:A : ARG1027:HH22: Lig: LIG1: O:	2.009
S8	-5.48	-0.17	95.71	-8.23	-	-	-
S9	-5.86	-0.18	50.94	-8.15	2	2xir:A : ASN923:HN: Lig: LIG1: O: 2xir:A: ASN923:HD21: Lig: LIG1: O:	1.675 1.721
S10	-7.43	-0.23	3.55	-10.05	3	2xir:A : ARG1027:HH22: Lig: LIG1: O: 2xir:A: ASP1046:HN: Lig: LIG1: O: 2xir:A:ILE1025:HN: Lig: LIG1: O:	2.164 2.039 2.109

View Article Online
DOI: 10.1039/C7MD00593H

Graphical abstract